Dual Targeting of Histone Deacetylases and MYC as Potential Treatment Strategy for H3-K27M Pediatric Gliomas

Danielle Algranati[1+], Roni Oren[2+], Bareket Dassa[3], Liat Fellus-Alyagor[2], Alexander Plotnikov[4], Haim Barr[4], Alon Harmelin[2], Nir London[5], Guy Ron[6], Noa Furth[1*] and Efrat Shema[1*]

[1]Department of Immunology and Regenerative Biology, Weizmann Institute of Science, Rehovot 76100, Israel.

[2]Department of Veterinary Resources, Weizmann Institute of Science, Rehovot 76100, Israel.

[3]Bioinformatics Unit, Department of Life Sciences Core Facilities, Faculty of Biochemistry, Weizmann Institute of Science, Rehovot 76100, Israel

[4]Wohl Institute for Drug Discovery of the Nancy and Stephen Grand Israel National Center for Personalized Medicine, Weizmann Institute of Science, Rehovot 76100, Israel

[5]Department of Chemical and Structural Biology, Weizmann Institute of Science, Rehovot 76100, Israel.

[6]Racah Institute of Physics, Hebrew University, Jerusalem 91904, Israel.

* Corresponding authors:

Efrat.shema@weizmann.ac.il

Noa.furth@weizmann.ac.il

[+] Equal contribution

Abstract

Diffuse midline gliomas (DMG) are aggressive and fatal pediatric tumors of the central nervous system that are highly resistant to treatments. Lysine to methionine substitution of residue 27 on histone H3 (H3-K27M) is a driver mutation in DMGs, reshaping the epigenetic landscape of these cells to promote tumorigenesis. H3-K27M gliomas are characterized by deregulation of histone acetylation and methylation pathways, as well as the oncogenic MYC pathway. In search of effective treatment, we examined the therapeutic potential of dual targeting of histone deacetylases (HDACs) and MYC in these tumors. Treatment of H3-K27M patient-derived cells with Sulfopin, an inhibitor shown to block MYC-driven tumors *in-vivo*, in combination with the HDAC inhibitor Vorinostat, resulted in substantial decrease in cell viability. Moreover, transcriptome and epigenome profiling revealed synergistic effect of this drug combination in downregulation of prominent oncogenic pathways such as mTOR. Finally, *in-vivo* studies of patient-derived orthotopic xenograft models showed significant tumor growth reduction in mice treated with the drug combination. These results highlight the combined treatment with PIN1 and HDAC inhibitors as a promising therapeutic approach for these aggressive tumors.

Introduction

Diffuse midline gliomas (DMGs) are fatal tumors of the central nervous system that occur primarily in children[1,2]. Years of clinical trials have revealed that conventional chemotherapy is ineffective, and with no option for complete resection, DMG is now the leading cause of brain tumor-related death in children[3,4]. Sequencing studies showed that up to 80% of the diagnosed children exhibit a lysine 27 to methionine (H3-K27M) mutation in one of the genes encoding histone H3.3 and H3.1 (clinically classified as DMG, H3 K27M–mutant). Numerous subsequent studies revealed pronounced alterations in the epigenetic landscape driven by this histone mutation[5–8]. Among these global epigenetic alterations are a drastic loss of H3 lysine 27 tri-methylation (H3K27me3), concomitant with an increase in H3 lysine 27 acetylation (H3K27ac). These epigenetic alterations were shown to affect transcriptional programs and support tumorigenesis [9–14].

Detailed characterization of the modes of chromatin deregulation in these tumors pointed toward targeting epigenetic pathways as a promising therapeutic approach[15]. Specifically, pervasive H3K27 acetylation patterns observed in H3-K27M DMGs, along with enrichment of H3K27ac specifically on mutant nucleosomes[11–13,16], underscored the histone acetylation pathway as a potential drug target for this cancer. Indeed, pan-histone deacetylase inhibitors (HDACi), such as Vorinostat and Panobinostat, were found to inhibit growth and to restore gene expression alterations observed in H3-K27M malignant gliomas[17–19]. However, recent studies demonstrated that H3-K27M cells develop resistance to HDACi treatment[17,19], stressing the importance of identifying novel drug combinations to induce synergistic inhibition of oncogenic pathways.

The MYC oncogenic pathway is frequently deregulated in diverse cancers, and thus stands as a prominent therapeutic target[20]. High-level gene amplification of *MYC* is recurrently observed in pediatric high-grade gliomas[21,22]. H3-K27M gliomas show high expression of *MYC* and MYC target genes, due to both epigenetic alterations and structural variants, resulting in a viability dependency on MYC signaling[12,23,24]. Unfortunately, directly targeting MYC in tumors is extremely challanging[25]. Dubiella et al. have recently developed a unique inhibitor targeting Peptidyl-prolyl isomerase NIMA-interacting-1 (PIN1), an upstream regulator of MYC activation[26]. PIN1 itself is frequently upregulated in many types of cancers, resulting in sustained proliferative signaling and tumor growth[27,28]. The PIN1 inhibitor, Sulfopin, was shown to downregulate MYC target genes *in-vitro* and to block MYC-driven tumors in murine models of neuroblastoma[26].

To address the increasing need for an effective combination therapy for H3-K27M DMGs, we tested whether dual targeting of histone acetylation and MYC activation, using Vorinostat and

Sulfopin, would yield beneficial outcome. We show that the combined treatment substantially reduces viability of patient-derived glioma cells, in concordance with inhibition of prominent oncogenic pathways, including the mTOR pathway. Treatment of H3-K27M DMG xenograft mice models with this drug combination led to reduced tumor growth and confirmed downregulation of mTOR *in-vivo*. Together, these results suggest the combination of PIN1 and HDAC inhibitors as a promising therapeutic strategy for H3-K27M gliomas.

Results

Sulfopin inhibits MYC targets and reduces viability of H3-K27M glioma cells

In light of the important role of MYC in H3-K27M DMGs, we set to explore whether the PIN1 inhibitor, Sulfopin, may affect MYC signaling in these cells and thus confer therapeutic potential. Sulfopin dependent inhibition of PIN1 was shown to downregulate the expression of MYC target genes in several cancer cell lines[26]. Indeed, RNA sequencing analysis of H3-K27M mutant patient-derived glioma cells (SU-DIPG13) treated with Sulfopin revealed strong enrichment of MYC targets among the downregulated genes (Fig. 1A). The genes downregulated by Sulfopin were also enriched for MYC-bound genes identified in several non-glioma cell lines, supporting a role for PIN1 in activation of the MYC pathway also in these glioma cells (Fig. S1A-B). Of note, Sulfopin was developed as a covalent inhibitor of PIN1, and did not lead to PIN1 degradation, as previously shown (Fig. S1C) [26]. We further validated the decreased expression of prominent MYC targets[27,29,30] upon Sulfopin treatment by RT-qPCR analysis (Fig. 1B, S1D). Interestingly, Cut&Run analysis[31] revealed an increase in H3K27me3 levels, indicative of repressed chromatin[32], around the transcriptional start sites (TSS) of MYC target genes, correlating with silencing of these genes upon PIN1 inhibition (Fig. 1C, S1E). Of note, global H3K27me3 distribution on all TSS and gene-body regions was not affected by Sulfopin treatment, supporting a specific increase in H3K27me3 on the TSS of MYC target genes (Fig. S1F-G). Furthermore, Sulfopin-unique H3K27me3 peaks (i.e., peaks that were found only in the Sulfopin-treated cells, and not in DMSO-treated cells) were enriched for MYC target genes (Fig. 1D).

We next explored the effect of Sulfopin on the viability of eight patient derived DMG cultures, harboring either the H3.3-K27M or H3.1-K27M mutation. Inhibition of PIN1 by Sulfopin was previously shown to delay cell cycle progression and thus reduce cell viability after extended treatments of 6-8 days [26]. In line with downregulation of MYC signaling, Sulfopin treatment led to a mild reduction in cell viability, conserved across the different cultures (Fig. 1E). To examine whether H3-K27M mutation renders DMG cells more sensitive to Sulfopin treatment, we took advantage of two sets of isogenic H3-K27M mutant patient-derived DMG cell-lines (SU-DIPG13, BT245) in which the *H3F3A*-K27M mutant allele has been knocked-out (KO).

86 In both lines, the reduction in cell viability was partially rescued in the KO cells (Fig. 1F),
87 suggesting higher sensitivity of H3-K27M mutant cells to MYC inhibition by Sulfopin. These
88 results are in line with previous reports showing H3-K27M-dependent activation of the
89 MYC/RAS axis in mouse and human cells[12,23,24]. Of note, DMG cells showed greater sensitivity
90 to the inhibitor compared to human astrocytic-like cells (Fig. S1H).

91 To further explore the status of MYC and PIN1 as indicators of response to Sulfopin inhibition,
92 we analyzed published transcriptomic dataset of DMG tumors[35]. Interestingly, while DMG
93 samples showed significantly higher expression of MYC and its target genes compared to
94 normal samples, PIN1 expression was lower in the cancer compared to matched normal tissue
95 (Fig. S1I-K). Furthermore, H3-K27M mutant tumors showed higher expression of MYC,
96 compared to H3 WT tumors, while PIN1 levels were reduced across samples[22] (Fig. S1L-M).
97 These results suggest that MYC expression levels, and not PIN1, may determine the sensitivity
98 of H3-K27M cells to Sulfopin treatment. To examine this notion, we measured the expression
99 levels of MYC, as well as the doubling time of the different DMG cultures. The response to
100 Sulfopin treatment (as reflected by IC50 measurements) correlated with the cells' doubling time
101 (Fig. S1N). Cells that divide faster were more sensitive to Sulfopin treatment, in line with PIN1
102 role in regulating cell cycle progression, and specifically G2/M transition[36,37]. As expected, the
103 doubling time negatively correlated with MYC expression, suggesting that MYC levels may
104 predict the response to Sulfopin (Fig S1O). Indeed, MYC levels negatively correlated with the
105 IC50 of Sulfopin; thus, cells relaying on high MYC activity showed higher sensitivity to
106 Sulfopin (Fig S1P).

107 H3K27me3 levels were shown to be drastically deregulated in DMG cells expressing H3-
108 K27M, with global loss of this modification across the genome, and retention of residual
109 H3K27me3 at CpG islands (CGIs). These residual H3K27me3 levels were shown to be
110 necessary to silence tumor suppressor genes and maintain cell proliferation in DMG cells[33,34] .
111 Interestingly, Sulfopin treatment resulted in reduction of H3K27me3 signal over CGIs, perhaps
112 contributing to Sulfopin-dependent growth inhibition in these cells (Fig. S1Q). Taken together,
113 our results indicate that PIN1 inhibition by Sulfopin downregulated MYC target genes, reduced
114 H3K27me3 levels at CGIs, and led to reduce viability of DMG cells in a H3-K27M-dependant
115 manner.

116 **Combination of Sulfopin and Vorinostat elicits robust inhibition of oncogenic pathways**
117 **and an additive effect on cell viability**

118 Inspired by the positive outcome of combinatorial drug therapy in H3-K27M DMG models[17,38],
119 we aimed to explore whether combining Sulfopin treatment with an epigenetic drug will further
120 reduce cell viability. H3-K27M gliomas are characterized by deregulation of epigenetic

121 pathways affecting post-translational modifications of lysine 27 (methylation and acetylation)
122 and lysine 4 (methylation) on histone H3[9–12,16,39]. Thus, we explored the effects of combining
123 sub-IC50 concentration of Sulfopin with four epigenetic inhibitors targeting critical
124 components associated with these modifications: (1) EPZ-6438, an inhibitor of EZH2, the
125 catalytic subunit of the PRC2 complex that deposits H3K27me3[40]. H3-K27M cells were
126 reported to be sensitive to EZH2 inhibition as they rely on the residual H3K27me3 levels to
127 suppress key tumor-suppressor genes[13,33,41,42]; (2) GSK-J4, an inhibitor of the H3K27me3
128 demethylase JMJD3[43], shown to rescue H3K27me3 levels in H3-K27M gliomas[17,44]; (3) MM-
129 102, an inhibitor of the H3K4me3 methyltransferase MLL1[40], shown to reduce viability of H3-
130 K27M-mutant cells[16]; and (4) Vorinostat, an HDAC inhibitor that was shown to have clinical
131 benefit in H3-K27M gliomas[17–19]. Treatment dosages of these drugs were set according to
132 previous studies [33,17,16]. We found that the combination of Sulfopin and Vorinostat (HDACi)
133 had the strongest effect, reducing viability by 80% (Fig. S2A).

134 Next, we adjusted treatment protocols to account for the optimal treatment period for each drug,
135 and examined the effect of this drug combination on the viability of eight H3-K27M mutant
136 patient-derived DMG cultures, across different dosages (Fig. 2A-B and S2B-D). For each pair
137 of concentrations, we calculated a BLISS index; an additive effect of the two drugs was
138 determined as BLISS index ~1[45,46] (Fig. 2C, S2E). While the combined treatment was effective
139 in all the cultures, cells harboring H3.3-K27M showed higher sensitivity (Fig. 2D, S2F).
140 Moreover, while an additive effect of Sulfopin and Vorinostat was detected in all the H3.3-
141 K27M DMG cultures in most of the drug doses, for the H3.1-K27M cultures we measured an
142 additive effect only in higher dosages of Vorinostat (Fig. 2C-E and S2E-F). In line with the
143 difference in sensitivity, H3.1- and H3.3-K27M cells differed substantially in MYC expression
144 levels, with H3.1-K27M cells expressing significantly lower levels of MYC (Fig. S2G). Indeed,
145 BLISS indexes negatively correlated with MYC expression levels (Fig. 2F), indicating that
146 H3.3-K27M cells, which express higher levels of MYC, are more sensitive to the combination
147 of Sulfopin and Vorinostat. Importantly, this highlights MYC, and MYC target genes, as
148 potential biomarkers of response for the combined treatment. For example, the expression
149 levels of the two MYC targets, NOC4L and PSMD3, negatively correlated with the BLISS
150 indexes and significantly differed between H3.1- and H3.3-K27M cells (Fig. 2F and S2H).
151 Furthermore, these and additional MYC targets were downregulated following the combined
152 treatment in the H3.3-K27M culture, SU-DIPG13 (Fig. S2I). Overall, our data demonstrates
153 that combining Sulfopin treatment with Vorinostat results in an additive effect on the viability
154 of DMG cultures, with H3.3-K27M cells showing higher sensitivity. This is in line with
155 previous studies highlighting clinical and molecular distinction between H3.1- and H3.3-K27M
156 mutant tumors, which is thought to dictate their targetable vulnerabilities[5,47,48].

157 To gain more insights on the molecular mechanisms underlying this effect on viability, we
158 profiled the transcriptome of SU-DIPG13 cells (H3.3-K27M) treated with each of the drugs
159 alone and the combined treatment (Fig. S2J). A total of 494 genes were significantly
160 differentially expressed (DE) in cells treated with the drug combination, compared to only 145
161 and 167 in cells treated solely with Sulfopin or Vorinostat, respectively (Fig. S2K-L).
162 Hierarchical clustering of all 620 DE genes confirmed strong additive effect of the combined
163 treatment on gene expression, primarily demonstrated by clusters 1 and 4 (Fig. 2G). Cluster 1,
164 consisting of approximately half of the DE genes, was strongly downregulated by the combined
165 treatment, compared to single-agent treated cells. This cluster included genes that play crucial
166 roles in glioma progression such as *MTOR*, *ATF3*, *CREB3 and TGFA*[49–52] (Fig. S2M).
167 Moreover, the mTORC1 signaling pathway was highly enriched within the genes comprising
168 cluster 1 (Fig. S2N). Importantly, GSEA analysis revealed that this pathway was significantly
169 enriched in downregulated genes following the combined treatment (Fig. 2H and S2O). Of note,
170 additional epigenetic and oncogenic pathways such as BMI1, cAMP and IL-6/JAK/STAT3
171 were significantly downregulated in cells treated with the drug combination[53–55] (Fig. 2I and
172 S2O). Reduction in mTOR signaling (mTOR, phospho-mTOR and phospho-S6[56]) and ATF3
173 was further validated by western blot and RT-qPCR analysis (Fig. 2J, S2P). Importantly, we
174 also confirmed that the combined treatment with Sulfopin and Vorinostat led to induction of
175 p21 (CDKN1A), a prominent tumor suppressor promoting cell cycle arrest and regulated by
176 mTOR signaling[57–59] (Fig. 2H, J). Finally, exploring mTOR expression in all the tested DMG
177 cultures, revealed a strong negative correlation with the BLISS indexes of the combined
178 treatment (Fig. S2Q), suggesting mTOR as a potential biomarker of response for the combined
179 treatment of Sulfopin and Vorinostat. Overall, our data revealed that the combined inhibition
180 of HDACs and MYC results in robust downregulation of prominent oncogenic pathways.

181 **Sulfopin attenuates HDACi-mediated accumulation of H3K27ac on genomic regions**
182 **associated with oncogenic pathways**

183 We next examined epigenetic features that may underly the inhibition of oncogenic pathways
184 by the combined treatment (keeping the same experimental set-up as shown in figure 2A).
185 Inhibition of histone deacetylases is expected to increase and alter genome-wide histone
186 acetylation patterns, including the H3K27ac mark associated with active promoters and
187 enhancers[60]. Indeed, global quantification by single-molecule measurements of H3K27-
188 acetylated nucleosomes, as well as western blot analysis, confirmed HDACi-mediated increase
189 in H3K27ac global levels (Fig. 3A-C, S3A). Interestingly, treatment with Sulfopin alone had
190 the opposite effect, reducing the percentage of acetylated nucleosomes (Fig. 3B-C, S3A). As
191 acetylation is coupled with transcription activation, this is in line with the function of Sulfopin
192 as an inhibitor of MYC transcriptional activity[26,61]. As a result, the global HDACi-mediated

193 increase in histone acetylation was also attenuated in the combined treatment with Sulfopin
194 (Fig. 3B-C, S3A).

195 To profile changes in the genomic distribution of H3K27ac and H3K27me3, we applied
196 Cut&Run in SU-DIPG13 cells treated with Vorinostat alone or in combination with Sulfopin.
197 We first examined the promoters of genes differentially expressed in the combined treatment
198 (as clustered in Fig. 2G). Genes comprising cluster 1 showed higher basal expression levels
199 compared to genes from cluster 4, and these expression differences were also reflected in higher
200 H3K27ac at these genes' promoters (Fig. S3B-C). Moreover, in accordance with the reduction
201 in RNA expression levels of genes comprising cluster 1, the combined treatment led to the
202 strongest local reduction of H3K27ac levels associated with their promoters (Fig. 3D).
203 Specifically, we found that several of the oncogenes that comprise cluster 1, such as mTOR,
204 and mTOR regulator-SLC7A5, RELB and COPB2, showed decreased levels of H3K27ac at
205 their promoters following the combined treatment[62–64] (Fig. 3E, S3D). Cluster 1 genes also
206 gained H3K27me3 on their promoters upon the combined treatment, supporting their epigenetic
207 repression following Sulfopin and Vorinostat treatment (Fig. S3E).

208 We further identified genomic regions in which histone acetylation is lost in a Sulfopin-
209 dependent manner (i.e., H3K27ac peaks that are present in Vorinostat-treated cells, but are lost
210 in the combined treatment with Sulfopin). Genome distribution analysis of these unique peaks
211 revealed that the majority of them localize to distal regions (Fig. S3F) and more than 60% of
212 them localize to annotated enhancers. Importantly, genes associated with these enhancers were
213 strongly enriched for oncogenic pathways such as RAS, MAPK and PI3K-AKT signaling
214 pathways[66–68] (Fig. 3F, S3G). Specifically, the combined treatment reduced H3K27ac levels on
215 several enhancers linked to genes involved in mTOR pathway and gliomagenesis, such as:
216 *AKT3*, *JAK1* and *NFKB2* genes, that were shown to have critical role in malignant gliomas[69–
217 73], *SEC13* gene that indirectly activates mTOR[74,75], and *CD93*, a key regulator in glioma[76] (Fig
218 3G and S3H). Concomitant with the lower H3K27ac levels associated with these enhancers, we
219 also observed lower expression of the associated genes (Fig. 3H and S3I). Taken together, the
220 results show attenuation of HDACi-mediated accumulation of H3K27ac levels upon combined
221 treatment with Sulfopin, associated with promoters and enhancers of prominent oncogenes.
222 This is in-line with reduced expression of these oncogenic pathways, strengthening the
223 therapeutic potential of the combined treatment.

224 **The combined treatment reduces tumor growth in a DMG xenograft mouse model**

225 Finally, we examined whether the combined inhibition of HDACs and PIN1 elicits an additive
226 effect also *in-vivo*. Thus, we established a H3-K27M DMG orthotopic xenograft model by
227 injections of SU-DIPG13P* cells, engineered to express firefly luciferase, to the pons of

228 immunodeficient mice[17]. Mice were given ten days to develop tumors, and then randomly
229 assigned to four groups: control mice treated with DMSO, mice treated with Sulfopin or
230 Vorinostat as single agents, and mice treated with the combination of Sulfopin and Vorinostat.
231 Both drugs were given daily and tumor growth was monitored by in *in-vivo* bioluminescence
232 imaging. In-line with our *in-vitro* results, we found significant reduction in tumor growth
233 following the combined treatment compared to control DMSO treated mice (Fig. 4A-B).
234 Importantly, the reduction was also seen when comparing to mice treated solely with
235 Vorinostat, supporting the additive value of Sulfopin to the well-known anti-tumorigenic effect
236 of HDACi in H3-K27M gliomas[17] (Fig. 4A-B). Of note, mice from all groups showed signs of
237 severe dehydration and general deterioration after 18 days of treatment, and thus we could not
238 measure a survival benefit for the combined treatment. This rapid deterioration is likely a result
239 of the aggressiveness of the transplanted tumors and does not represent side effects of the
240 treatment, as mice from all groups, including the non-treated mice, showed similar signs of
241 deterioration.

242 To link our *in-vitro* transcriptomic analysis to the *in-vivo* effect on tumor growth, we assessed
243 the percentage of H3-K27M cells that are positive to mTOR signal (double-positive), out of the
244 total number of H3-K27M cells, by immunofluorescence staining. The combined treatment
245 significantly reduced the fraction of the double-positive cells, compared to DMSO (Fig. 4C-D).
246 Of note, mTOR signal in the mouse cells surrounding the tumor showed no significant
247 differences between the DMSO and the combination-treated mice (Fig S4A-B). Overall, these
248 results verify the potency of this treatment in restricting oncogenic pathways also *in-vivo*, and
249 the potential clinical benefit of PIN1 and HDAC combined inhibition in H3-K27M-mutant
250 DMGs.

251 **Discussion**

252 Despite decades of efforts to improve treatment for children diagnosed with H3-K27M-mutant
253 DMGs, the standard of care remains solely radiation, with no significant improvement in
254 overall survival[1,2,79]. High throughput drug screens in patient-derived cells identified HDAC
255 inhibition as a promising therapeutic strategy, and ongoing clinical trials revealed preliminary
256 evidence of clinical benefit[38,80] (NCT02717455, NCT03566199). However, emerging
257 resistance to HDACi in glioma cells[17], as well as limited therapeutic benefits of HDACi
258 treatment as a sole agent[81,82], highlight the necessity to discover additional therapy modalities
259 that could prolong survival and relieve symptoms.

260 In H3-K27M-mutant DMGs, as well as in many other malignancies, high MYC activity is
261 correlated with poor prognosis and therefore considered as an attractive therapeutic target[21,83].
262 Nevertheless, direct targeting of MYC is highly challenging, functional and structural wise.

263 MYC signaling, while amplified in cancer cells, is also essential to normal cell function[84].
264 Moreover, as a transcription factor, MYC lacks traditionally druggable binding pockets,
265 hindering the development of direct small molecule binders[25]. To overcome this, in this study
266 we exploited Sulfopin, a novel, potent and selective PIN1 inhibitor[26]. Pre-clinical studies have
267 shown *in-vivo* activity and negligible toxicity of Sulfopin in murine models of PDAC and
268 neuroblastoma[26]. While PIN1 is not overexpressed in DMG tumors, we show that Sulfopin,
269 although not inhibiting MYC directly, downregulates MYC target genes in patient-derived
270 DMG cells and affects cell survival in a H3-K27M-dependant manner. These results are in line
271 with the contribution of MYC signaling to H3-K27M-driven tumorigenesis[23,24], underscoring
272 the therapeutic potential of Sulfopin for these aggressive brain tumors. Notably, despite a
273 significant reduction in tumor size in-vivo, the combined treatment did not increase mice
274 survival. This is perhaps due to the relatively large tumors already formed at the onset of
275 treatment, leading to rapid deterioration of mice in all experimental groups. Thus, further
276 optimization of the modeling system and therapeutic regime is needed.

277 We showed that combining Sulfopin treatment with the HDAC inhibitor Vorinostat reduced
278 cell viability by 80% in several tumor-derived DMG lines originating from different patients.
279 Importantly, the combination resulted in an additive effect not only on cell viability, but also
280 on transcriptional programs. A key oncogenic pathway that was robustly downregulated in the
281 combined treatment, *in-vitro* and *in-vivo,* is the mTOR signaling pathway. Preclinical and
282 clinical data support a role for mTOR in gliomagenesis[85]. Specifically, AKT gain or PTEN loss
283 is detected in approximately 70% of DMG tumors, and a recent study showed high expression
284 of mTOR in DMGs. Thus, the PTEN/AKT/mTOR pathway is suggested to play a key role in
285 this disease[86–89]. Attempts to restrict mTOR signaling using first generation mTOR inhibitors
286 primarily inhibited mTORC1, which often caused upregulation of mTORC2[90]. The combined
287 treatment with Sulfopin and Vorinostat led to robust inhibition of several target proteins in the
288 mTOR signaling pathway, likely via alternative pathways. One potential candidate is the
289 mTOR-dependent cell-growth through MYC regulation, which may be impaired by Sulfopin
290 treatment, inhibiting MYC transcriptional activity[91–94]. Of note, drug agents targeting both
291 mTORC1 and mTORC2 were shown to be highly effective in DMG cells as well as in murine
292 models[95,96].

293 Expression of the H3-K27M oncohistone is associated with a prominent increase in H3K27ac
294 levels[11–13,16]. Among the loci that accumulate this modification are repetitive elements and
295 endogenous retroviruses (ERVs), resulting in their aberrant expression, potentially inducing
296 innate immune responses[12]. However, H3-K27M cells do not show an increase in interferon
297 stimulated genes (ISGs), preassembly due to high levels of MYC, which is potent antagonist of
298 interferon responses[12,97]. Thus, dual targeting of both HDAC and MYC pathways has the

potential of inducing robust expression of ISGs, thus promoting tumor cell death mediated by viral-mimicry[98].

The high levels of H3K27ac in H3-K27M cells was also linked to activation of super-enhancers, which regulate the expression of oncogenes and genes that are associated with an undifferentiated state[79]. Here, we show that H3-K27M cells are vulnerable to transcriptional disruption mediated by the combined treatment with Sulfopin and Vorinostat. While treating cells with Vorinostat alone increased H3K27ac levels, as expected, the combined treatment attenuated the accumulation of this mark on promoters and enhancers of prominent oncogenes, resulting in their decreased expression. This Sulfopin-mediated attenuation could potentially result from downregulation of MYC targets, as it was recently shown that MYC overexpression results in H3K27ac gain on super-enhancers[99].

In summary, we propose a novel therapeutic strategy targeting epigenetic and transcriptional pathways in H3-K27M-mutant DMG tumors. HDAC inhibition, in combination with the novel MYC inhibitor, inhibited oncogenic transcriptional signatures and reduced tumor growth *in-vivo*. Our findings emphasize epigenetic dependencies of H3-K27M driven gliomas and highlight the therapeutic potential of combined treatments for this aggressive malignancy.

Acknowledgments

We thank H. Keren-Shaul, D. Robbins, Y. Elazari and N. Adler (G-INCPM, WIS) for their help with NGS; N. Morris for her help with conducting part of the cell viability assays; C. Raanan, and M. Zerbib for their contribution in establishing the DIPG mouse model; I. Savchenko for his help with immunohistochemistry; R. Gabizon for generously providing Sulfopin for *in-vitro* and *in-vivo* experiments and helping with Sulfopin handling; S. Fishilevich for providing the GeneHancers data; L. Segev for computational framework for single-molecule image analysis; N. Harpaz and O. Beresh for helping with cultures maintenance; O. Griess for helping with transcriptomic protocols; S. Gillespie for providing valid information on DMG cells growth and maintenance; and I. Ulitsky for providing the pAG-MNase enzyme. We are thankful to O. Golani for helping with the immunohistochemistry image analysis. We are grateful to M. Monje for generously sharing with us the SU-DIPG13, SU-DIPG13P*, SU-DIPG6, SU-DIPG17, SU-DIPG25, SU-DIPG36, SU-DIPG38, SU-DIPG21 and SU-DIPG50 cells. We are grateful to N. Jabado for her kind gift of the isogenic BT245 and SU-DIPG13 cultures. We would like to express our sincere gratitude to D. Deitch for producing part of the graphs, designing the figures and illustrations, and helping with statistical analysis. **Funding:** E.S. is an incumbent of the Lisa and Jeffrey Aronin Family Career Development chair and is also supported by Henry Chanoch Krenter Institute for Biomedical Imaging and Genomics. This research was supported by grants from the European Research Council (ERC801655), The Israel Science Foundation

(1881/19), Emerson Collective, and The Israel Cancer Research Fund: Research Career Development Award.

Author contributions

D.A, N.F and E.S. designed the study and wrote the manuscript; D.A conducted the experiments; R.O and A.H established the xenograft mice model and performed *in-vivo* experiments; B.D, D.A, N.F and E.S performed bioinformatics analysis. L.F.A, R.O, G.R and D.A conducted the *in-vivo* image analysis; H.B and A.P conducted part of the viability assays; N.L suggested and provided Sulfopin and valuable usage information.

Declaration of interests

N.L. is an inventor on a patent describing Sulfopin (US 2021/0332024 A1).

344 **Figure legends**

345 **Figure 1: Sulfopin inhibits MYC signaling and reduces viability of DMG cells in a H3-**
346 **K27M-dependent manner**

347 (A) Functional enrichment analysis on significantly downregulated genes in SU-DIPG13 cells
348 treated with 10uM Sulfopin for 12 hours, compared to DMSO. Enrichr algorithm[123] was used
349 to compare downregulated genes against the Molecular Signatures Database (MSigDB)
350 hallmark geneset[119]. Dashed line denotes adjusted p-value = 0.05. MYC targets are significantly
351 enriched among the Sulfopin downregulated genes.

352 (B) RT-qPCR analysis of selected MYC target genes in SU-DIPG13 cells treated with 10uM
353 Sulfopin for 12 hours, compared to DMSO. Fold change between Sulfopin and DMSO treated
354 cells was calculated and the mean ± SD of two technical repeats is shown.

355 (C) H3K27me3 Cut&Run read coverage over MYC target genes ('MYC Targets V1' hallmark
356 geneset[119], n=200), in SU-DIPG13 cells treated with 10uM Sulfopin for 8 days compared to
357 DMSO. Sulfopin treatment increases H3K27me3 levels on the TSS of MYC target genes.

358 (D) Functional enrichment analysis of the genes associated with Sulfopin-unique H3K27me3
359 peaks, in SU-DIPG13 cells treated as in C. Dashed line denotes adjusted p-value = 0.05. MYC
360 target geneset ('MYC Targets V1' hallmark geneset[119]) is mildly enriched among these genes,
361 with adjusted p-value of 0.077.

362 (E) Cell viability, as measured by CellTiterGlo, of eight DMG cultures (H3.3K27M: SU-
363 DIPG13, SU-DIPG6, SU-DIPG17, SU-DIPG25 and SU-DIPG50. H3.1K27M: SU-DIPG36,
364 SU-DIPG38 and SU-DIPG21), treated with Sulfopin for eight days with pulse at day four,
365 compared to DMSO. Mean±SD of two technical replicates is shown. Logarithmic scale is used
366 for the x-axis. Sulfopin treatment led to a mild reduction in cell viability in all H3-K27M glioma
367 cultures.

368 (F) Cell viability, as measured by CellTiterGlo, of two isogenic DMG cell lines (SU-DIPG13
369 and BT245) in which the mutant histone was knocked-out (KO), treated with the indicated
370 concentration of Sulfopin for 8 days, compared to DMSO. For each cell line and concentration,
371 the fold change in viability between Sulfopin and DMSO treated cells is shown. For SU-
372 DIPG13-mean ± SE of at least two independent experiments is shown. For BT245-mean± SD
373 of three technical replicates is shown. H3-K27M glioma cells show higher sensitivity to
374 Sulfopin treatment compared to the KO cells. *P < 0.05; **P < 0.01 (two-sample t-test over all
375 technical replicates). Significance adjusted after Bonferroni correction.

376

377 **Figure 2: Combination of Sulfopin and Vorinostat elicits robust downregulation of**
378 **oncogenic pathways**

379 (A) Timeline demonstrating the treatment protocol for the combination of Sulfopin and
380 Vorinostat.

381 (B) Percentage of cell viability, as measured by CellTiterGlo of SU-DIPG13 cells treated with
382 Sulfopin and Vorinostat at the indicated concentrations, compared to DMSO.

383 (C) BLISS index measured as the ratio between the observed and the expected effect of the
384 combination of Sulfopin and Vorinostat, for each pair of concentrations, in SU-DIPG13.
385 Synergy: Bliss <1 ,Additive: Bliss=1, Antagonist: Bliss>1.

386 (D) Cell viability as measured by CellTiterGlo, of eight DMG cultures treated with Sulfopin
387 (0uM, 2.5uM, 5uM, 10uM, 20uM and 40uM) and Vorinostat (1uM), compared to DMSO.
388 H3.3-K27M and H3.1-K27M cultures are indicated in blue and orange, respectively. Mean±SD
389 of two technical replicates is shown. H3.3-K27M cells showed higher sensitivity to the
390 combined treatment compared to H3.1-K27M cells.

391 (E) The BLISS index of the combination of Sulfopin (10uM) and Vorinostat (1uM), in the
392 indicated cultures. An additive effect was detected in all the H3.3-K27M cultures at this set of
393 concentrations.

394 (F) Pearson correlation coefficient matrix of BLISS index of the combined treatment (Sulfopin
395 (10uM) and Vorinostat (1uM)) and mRNA levels of MYC and its target genes, in the eight
396 DMG cultures tested. mRNA levels were measured by RT-qPCR (Fig. S2F-G). Blue and yellow
397 colors indicate negative or positive correlation, respectively. Negative correlation was detected
398 between the BLISS indexes and the expression levels of MYC and its target genes.

399 (G) Unsupervised hierarchical clustering of expression levels of 620 significantly DE genes
400 detected in SU-DIPG13 cells treated with either Sulfopin (10uM, 8 days), Vorinostat (1uM, 72
401 hours), the combination of Sulfopin and Vorinostat or DMSO. Gene expression rld values (log2
402 transformed and normalized) were standardized for each gene (row) across all samples. Color
403 intensity corresponds to the standardized expression, low (blue) to high (red). Clusters 1 and 4
404 demonstrate additive transcriptional patterns associated with the combined treatment.

405 (H) Top: Gene Set Enrichment Analysis (GSEA) on SU-DIPG13 treated with combination of
406 10uM Sulfopin and 1uM Vorinostat compared to DMSO, showing significant downregulation
407 of mTORC1 signaling ('HALLMARK_MTORC1_SIGNALING' geneset[119]) in the combined
408 treatment. NES: Normalized Enrichment Score. FDR: false discovery rate. Bottom: Expression
409 levels of significantly DE genes detected in the combined treatment compared to DMSO that

410 are part of the mTORC1 signaling geneset. *MTOR* gene was added manually to the heat-map.
411 Heatmaps were generated as described in B.

412 (I) Top: Gene Set Enrichment Analysis (GSEA) on SU-DIPG13 treated as in C, showing
413 significant downregulation of the epigenetic BMI-1 pathway and the oncogenic cAMP pathway
414 in the combined treatment (BMI1_DN.V1_UP; CAMP_UP.V1_UP; MSigDB C6 oncogenic
415 signature[120,121]). Bottom: Expression levels of significantly DE genes detected in the combined
416 treatment compared to DMSO that are part of the BMI-1 and cAMP genesets. Heatmaps were
417 generated as in described B.

418 (J) Western blot of SU-DIPG13 treated either with Sulfopin (10uM, 8 days), Vorinostat (1uM,
419 72 hours), the combination of Sulfopin and Vorinostat or DMSO, using the indicated
420 antibodies. β-tubulin is used as loading control.

421

422 **Figure 3: The combined treatment attenuates H3K27ac levels on oncogenic targets**

423 (A) Scheme of the single-molecule imaging experimental setup[133]: cell-derived mono-
424 nucleosomes are anchored in a spatially distributed manner on polyethylene glycol (PEG)-
425 coated surface. Captured nucleosomes are incubated with fluorescently labeled antibodies
426 directed against the H3K27ac modification. Total internal reflection fluorescence (TIRF)
427 microscopy is utilized to record the position and modification state of each nucleosome. Time
428 series images are taken to allow detection of maximal binding events.

429 (B) Single-molecule imaging quantification of the percentage of H3K27ac nucleosomes, in SU-
430 DIPG13 cells treated with either Sulfopin (10uM, 8 days), Vorinostat (1uM, 72 hours), or the
431 combination of Sulfopin and Vorinostat, normalized to DMSO. Mean fold ± SE of at least two
432 independent experiments is shown. H3K27ac global levels are lower in the combined treatment
433 compared to cells treated solely with Vorinostat. *$P < 0.05$ (two sample t-test).

434 (C) SU-DIPG13 cells were treated as in B, and analyzed by western blot using the indicated
435 antibodies.

436 (D) Left panel: Heatmap shows H3K27ac read coverage around the TSS (+/-5Kb) of the
437 significantly DE genes shown in figure 2B, in SU-DIPG13 cells treated with the combination
438 of 10uM Sulfopin and 1uM Vorinostat versus DMSO. Average coverage is shown on top. Color
439 intensity corresponds to the standardized expression. Clusters 1-4 are indicated. Right panel:
440 The log2 ratio of H3K27ac read coverage in SU-DIPG13 cells treated with the combination of
441 10uM Sulfopin and 1uM Vorinostat vs. DMSO was calculated. Heatmap shows the ratio around
442 the TSS (+/-5Kb) of the significantly DE genes shown in figure 2B, and average coverage is
443 shown on top. Color intensity corresponds to the ratio between samples, low (red) to high
444 (blue). Clusters 1-4 are indicated, with cluster 1 presenting the strongest local decrease in
445 H3K27ac following the combined treatment compared to DMSO.

446 (E) IGV tracks of *MTOR* and *SLC7A5* gene promoters, showing H3K27ac coverage in SU-
447 DIPG13 cells treated as indicated.

448 (F) Functional enrichment analysis of the genes linked to enhancers (top targets of high
449 confident enhancers) marked with H3K27ac exclusively in SU-DIPG13 cells treated with
450 Vorinostat, and not in the combined treatment. gProfiler algorithm[126] was used to calculate
451 enrichment against the KEGG pathways DB[128]. Dashed line denotes adjusted p-value = 0.05.
452 Genes associated with Vorinostat-unique enhancers are enriched for oncogenic signaling
453 pathways.

454 (G) IGV track of *AKT3* and *SEC13* linked enhancers, showing H3K27ac coverage in SU-
455 DIPG13 cells treated with 1uM Vorinostat or the combination of 10uM Sulfopin and 1uM
456 Vorinostat.

457 (H) Normalized expression levels of *AKT3* and *SEC13* genes in SU-DIPG13 cells treated as in
458 G. Mean ± SD of three technical repeats is shown .*$P < 0.05$ (two-sample t-test).

459

460 **Figure 4: The combined treatment with Sulfopin and Vorinostat reduces tumor growth**
461 ***in-vivo***

462 (A-B) SU-DIPG13P* cells were injected to the pons of immunodeficient mice to form tumors.
463 Ten days post injection, mice were treated for 18 days with either DMSO, Sulfopin, Vorinostat,
464 or the combination of Sulfopin and Vorinostat. (A) *In-vivo* bioluminescent imaging of DMG
465 xenografts following 18 days of treatment. The heat map superimposed over the mouse head
466 represents the degree of photon emission by DMG cells expressing firefly luciferase. (B) DMG
467 xenograft tumor growth as measured by change in bioluminescent photon emission following
468 15 days of treatment with either DMSO (n=8), Sulfopin (n=4), Vorinostat (n=5) or the
469 combination of Sulfopin and Vorinostat (n=6). Data points represent the fold-change in
470 maximum photon flux between day 3 and day 18 under treatment for each mouse. *$P < 0.05$
471 (two-tailed Mann-Whitney U-test).

472 (C-D) Immunofluorescent staining of brain sections from mice treated with DMSO (n=4) or
473 the combination of Sulfopin and Vorinostat (n=4). (C) Representative fluorescence images of
474 H3-K27M (red) and mTOR (green). (D) Percentage of mTOR positive cells out of the total H3-
475 K27M-positive cells (n=13-198 cells per FOV). H3-K27M positive cells show lower levels of
476 mTOR following the combined treatment compared to DMSO. *$P < 0.05$ (two-tailed t-test).

477 478 **Methods**

479 **Data availability**

480 All sequencing data is deposited in NCBI's Gene Expression Omnibus (GEO) and available
481 through GEO series accession number GSE221614.

482 **Cell cultures**

483 All cell lines were maintained at 37°C with 5% CO2. Exclusion of Mycoplasma contamination
484 was monitored and conducted by test with EZ-PCR kit (Biological Industries # 20-700-20).

485 **Glioma cultures**

486 DIPG derived cells, SU-DIPG13 (H3.3-K27M, female), SU-DIPG6 (H3.3-K27M, female), SU-
487 DIPG17 (H3.3-K27M, male), SU-DIPG25 (H3.3-K27M, female), SU-DIPG50 (H3.3-K27M,
488 sex unknown), SU-DIPG36 (H3.1-K27M, female), SU-DIPG38 (H3.1-K27M, female), SU-
489 DIPG21 (H3.1-K27M, male) and SU-DIPG13P* were generated in the lab of Dr. Michelle
490 Monje, Stanford University[17]. SU-DIPG13P* are a subclone of the patient-derived SU-DIPG13
491 pons culture that demonstrates more aggressive growth in vivo[38,79].

492 K27M-KO SU-DIPG13, BT245-KO (sex information is unavailable) and corresponding
493 control clones were generated in the lab of Prof. Nada Jabado, McGill University, as previously
494 described by Krug et al[12].

495 Cells were cultured in Tumor Stem Media (TSM) consisting of a 1:1 mixture of DMEM/F12
496 (Invitrogen, 31330038) and Neurobasal -A (Invitrogen, 10888022) media, with 1:100 addition
497 of HEPES Buffer Solution (Invitrogen 15630-080), MEM Sodium Pyruvate Solution
498 (Invitrogen, 11360-070), MEM Non-Essential Amino Acids Solution (Invitrogen, 11140-050),
499 GlutaMAX-I (Invitrogen, 35050-061) and Antibiotic-Antimycotic (Invitrogen,15240-096).
500 The following additive were added freshly: B27 -A (1:50, Invitrogen, 12587010), human FGF
501 (20 ng/ml, Shenandoah Biotechnology, 100-146), human EGF (20 ng/ml, Shenandoah
502 Biotechnology, 100-26), human PDGF-AA (20 ng/ml, Shenandoah Biotechnology, 100-16),
503 human PDGF-BB (20 ng/ml, 100-18, Shenandoah Biotechnology) and heparin (10 ng/ml,
504 Stemcell Technologies, 07980). Doubling times were computed using: http://www.doubling-
505 time.com/compute.php.

506 **Astrocytic-like cells culture**

507 CRL-1718 cells, an astrocytic-like cells isolated from the brain of patient with astrocytoma
508 were kindly provided by Dr. D. Michaelson, Tel-Aviv University, Israel. Cells were cultured
509 in RPMI media (Biological Industries, # 01-101-1A) supplemented with 10% heat inactivated

510 Fetal Bovine Serum (FBS), 1 mM L-glutamine and 1% penicillin/streptomycin solution (all
511 from Biological Industries).

512 **Isolation of total RNA, reverse transcription and RT-qPCR**

513 RNA was isolated from 2 million cells using the NucleoSpin kit (Macherey Nagel,
514 #740955.50). 1ug of each RNA sample was reverse-transcribed using Moloney Murine
515 Leukemia Virus reverse transcriptase (M-MLV-RT, Promega, #M1701) and random hexamer
516 primers (Thermo Scientific, #SO142). Real-time qPCR was performed using KAPA SYBR
517 FAST mix (Kapa Biosystems, #KK4660) with a StepOne real-time PCR instrument (Applied
518 Biosystems). For each gene, standard curve was determined and the relative quantity was
519 normalized to GAPDH mRNA (Table S2).

520 **Isolation of total RNA, bulk MARS-Seq library preparation and sequencing**

521 RNA was isolated from SU-DIPG cells treated as indicated in Table S4a, using the NucleoSpin
522 kit (Macherey Nagel, 740955). A bulk adaptation of the MARS-Seq protocol[100,101] was used to
523 generate RNA-Seq libraries for expression profiling. Briefly, 30 ng of input RNA from each
524 sample was barcoded during reverse transcription and pooled. Following Agencourct Ampure
525 XP beads cleanup (Beckman Coulter, A63880), the pooled samples underwent second strand
526 synthesis and were linearly amplified by T7 in vitro transcription. The resulting RNA was
527 fragmented and converted into a sequencing-ready library by tagging the samples with Illumina
528 sequences during ligation, RT, and PCR. Libraries were quantified by Qubit (ThermoFisher
529 Scientific) and TapeStation (Agilent) as well as by qPCR for GAPDH housekeeping gene as
530 described below. Sequencing was done on a Nextseq 75 cycles high output kit (Illumina,
531 20024906).

532 **Bulk MARS-seq analysis**

533 A median of 10.5 to 20 million reads were obtained for each dataset (Table S4a). MARS-seq
534 analysis was preformed using the UTAP transcriptome analysis pipeline[113]. Reads were
535 trimmed to remove adapters and low quality bases using cutadapt[105] and mapped to the human
536 genome (hg38, UCSC) using STAR v2.4.2a18[114] (parameters: –alignEndsType EndToEnd, –
537 outFilterMismatchNoverLmax 0.05, –twopassMode Basic, –alignSoftClipAtReferenceEnds
538 No). In short, the pipeline quantifies the 3' of annotated genes (The 3' region contains 1,000
539 bases upstream of the 3' end and 100 bases downstream). Counting was done using HTSeq-
540 count in union mode[115]. Genes having a minimum 5 UMI-corrected reads in at least one sample,
541 were considered. Normalization of the counts and differential expression analysis was done
542 using DESeq2[116], and is provided in Table S4b-c (parameters: betaPrior=True,
543 cooksCutoff=FALSE, independentFiltering=FALSE). Significantly differentially expressed
544 genes were defined having adjusted p-value (with Benjamini and Hochberg procedure) <= 0.05,

545 |log2FoldChange| >= 1 and baseMean >= 5. Heatmaps of gene expression were calculated using
546 the log-normalized expression values (rld), with row standardization (scaling the mean of a row
547 to zero, with standard deviation of 1). Clustering of gene expression (rld values) was done using
548 Euclidian average linkage method, and visualized using Partek Genomics Suite 7.0 software
549 (Partek Inc. 2020. Partek® Genomics Suite®, Version 7.0). Boxplot was used to visualize gene
550 expression values (rld) of each differentially expressed gene from clusters 1 and 4 (in each of
551 the three replicates).

552 **Expression analysis from published data-sets**

553 Gene expression data and histone mutation status of pediatric high grade gliomas[22] was
554 downloaded from PedcBioPortal (https://pedcbioportal.kidsfirstdrc.org/). For matched tumor-
555 normal samples, RPKM values were obtain from Berlow et al[35] (S2_Table). For boxplots the
556 log2 (RPKM+1) or z-score values were used (ggpubr R package). Differences between groups
557 were assessed using two-sided 't_test' (rstatix R package). For heatmaps, gene expression
558 values were obtained for genes from MsigDB signatures
559 'HALLMARK_MYC_TARGETS_V1', with MYC and PIN1 genes added manually.
560 Heatmaps of gene expression were calculated using RPKM values, with row standardization
561 (scaling the mean of a row to zero, with standard deviation of 1).

562 **Functional enrichment analysis**

563 Gene set enrichment analysis (GSEA) was performed as described in
564 www.broadinstitute.org/software/gsea[117,118]. Genes detected by MARS-seq were pre-ranked
565 according to their fold change (log2) in Sulfopin+Vorinostat vs. DMSO treated cells. Pre-
566 ranked GSEA was applied using the Human MSigDB Collections H: hallmark gene sets[119], and
567 the C6: oncogenic signature gene sets[120–122]. Significantly downregulated gene-sets were
568 selected using cut-off of FDR q-value ≤ 0.1.

569 Enrichr algorithm[123] was used to compare significantly downregulated genes detected in the
570 different treatments, against one or more of the following databases: the Molecular Signatures
571 Database (MSigDB) hallmark[119], ChEA[124] or ENCODE TF ChIP[125].

572 gProfiler algorithm[126] was used to analyze genes that are putative targets of elite enhancers
573 which overlap with Vorinostat-unique H3K27ac peaks (see Cut&Run analysis), against the
574 KEGG[127,128] or Wiki[129] pathways databases.

575 **Cut&Run pulldown assay followed by high-throughput sequencing**

576 Cut&Run assay was done as described in Skene and Henikoff, 2017[31,102] with slight
577 modifications as follows: Cells were harvested and counted, with 200,000 cells taken per
578 reaction. Permeabilized cells, bound to Concanavalin A-coated beads (Bangs Laboratories,

579 BP531), were mixed with individual primary antibody (Table S1) and incubated overnight at
580 4°C while rotating. Secondary antibody, anti-rabbit HRP, was used as a negative control. pAG-
581 MNase enzyme (generated in the Department of Life Sciences Core Facilities, WIS, using
582 Addgene plasmid 123461) was added to each sample followed by incubation step of 1 h at 4°C.
583 Targeted digestion was done by 15 min incubation on ice block (0°C) under low salt conditions.
584 DNA purification was done using Nucleospin gel and PCR clean-up kit (Machery-Nagel,
585 740609).

586 Libraries were prepared from 1-20ng of DNA as previously described in Blecher-Gonen et al[103].
587 Briefly, DNA Fragments were repaired by T4 DNA polymerase (NEB, M0203), and T4
588 polynucleotide kinase (T4 PNK, NEB, M0201) was used to add a phosphate group at the 5′
589 ends. An adenosine base was then added by Klenow fragments (NEB, M0212) to allow efficient
590 ligation, using T4 quick ligase (NEB, M2200), of sequencing adapters, which contain a T-
591 overhang. DNA fragments were amplified by PCR reaction (Pfu Ultra II fusion, Agilent
592 Technologies, 600670), which also introduced the Illumina-P5 adapter at one end of the
593 molecule. SPRI beads were used to purify proper sized DNA fragments after each enzymatic
594 step. Libraries were quantified by Qubit (ThermoFisher Scientific) and proper fragment range
595 (200-400bp) was verified by TapeStation (Agilent). Sequencing was done on a Next-Seq 500
596 instrument (Illumina, #20024904) using a V2 150 cycles mid output kit (paired end
597 sequencing).

598 Paired-end reads of each sample (~7.5M median reads per sample, Table S5) were preprocessed
599 with cutadapt[105], to remove adapters and low-quality bases (parameters: --times 2 -q 30 -m 20),
600 following evaluation of quality with FastQC. Reads were mapped to human genome (hg38,
601 UCSC) using Bowtie version 2.3.5.1[106] (--local --very-sensitive-local --no-unal --no-mixed --
602 no-discordant --dovetail -I 10 -X 700). Nucleosome fragments at the length >120bp were
603 selected from the remaining unique reads using picard-tools, and broad peaks were called using
604 MACS2 against the HRP samples as background control (parameters: -f BAMPE --SPMR --
605 nomodel --extsize 100 --keep-dup auto -q 0.05). Analysis of genomic features was done using
606 ChIPseeker[107]. Reads coverage on TSS, gene body regions, specific gene-signatures and CGI
607 were visualized using ngs.plot[108]. Annotation of CGI were downloaded for UCSC table
608 browser. Association of peaks with specific genes was done using GREAT[109]. Bigwig files
609 were constructed from BAM alignments using deepTools2 suite[110], by 'bamCoverage'
610 command, using RPKM-normalization in 10bp bins. Heatmaps and profiles were constructed
611 in 'scale-regions' mode around peak summits, with missingDataAsZero paramter using
612 'plotHeatmap' and 'plotProfile' commands. In the heatmap of H3K27ac ratio (Fig. 3D)
613 coverage was calculated as the log2 between treatment and DMSO, on TSS of genes which
614 were depicted as differentially expressed by MARS-Seq. RPKM-normalized coverage files

615 were visualized on the genome using IGV (2.8.6). H3K27ac peaks were further distinguished
616 into Vorinostat-unique peaks (i.e., H3K27ac peaks that are present in Vorinostat-treated cells,
617 but are lost in the combined treatment with Sulfopin), and to shared peaks (i.e., H3K27ac peaks
618 that are present both in Vorinostat and in Sulfopin+Vorinostat treated cells, with a minimum of
619 1bp overlap) using bedtools[111]. H3K27me3 peaks unique to Sulfopin treatment were defined
620 similarly. To detect the overlap between the Vorinostat-unique peaks with enhancer regions,
621 we used the GeneHancer database v5.9[112]. We required a 30% overlap of the peak length with
622 a known enhancer categorized as "Elite" group, and excluded enhancers annotated to promoters
623 regions.

624 **Cell viability assay by CelltiterGlo**

625 For Sulfopin and Vorinostat combination experiments, 384-well plates were pre-plated with 2-
626 fold dilution matrix of Vorinostat (MCE Cat#HY-10221) and Sulfopin (generous gift from Dr.
627 Nir London's Lab, Weizmann institute of science), in 5 concentrations ranging from 120 to
628 10,000 nM (Vorinostat) and 2500 to 40,000 nM (Sulfopin). 1400 DIPG cells/well were plated
629 into each well containing 75ul of growth media, and subjected to drug treatment for 3 days
630 (Vorinostat) or 8 days with pulse at day 4 (Sulfopin). Single agent titrations were run in parallel.
631 Following the treatment, cells were subjected to cell viability assay using CellTiter-Glo assay
632 (# G7572, Promega, USA) in accordance to the manufacture protocol. Luminescence signal
633 was detected by luminescence module of PheraStar FS plate reader (BMG Labtech, Ortenberg,
634 Germany). Viability data was analyzed using GeneData 15 (Switzerland).

635 For generating Sulfopin dosage curves in DIPG versus Astrocytes cells, the appropriated
636 amounts of Sulfopin or DMSO (control) were transferred using Echo Liquid Handler 550
637 (Beckman, USA) into white/white 384-well TC plate (Greiner, #781080). 1400 cells/well were
638 dispensed by MultiDrop 384 dispenser (Thermo Scientific, USA) into 384-well plates. After 4
639 days, cells were subjected to cell viability assay using CellTiter-Glo assay (# G7572, Promega,
640 USA) in accordance to the manufacture protocol. Luminescence signal was detected by
641 luminescence module of PheraStar FS plate reader (BMG Labtech, Ortenberg, Germany).
642 Viability data was analyzed using GeneData 15 (Switzerland).

643 For all the other viability assays, cells were plated at a density of 2500 cells/well in 96-well
644 plates and subjected to drug treatment for 3 days (Vorinostat-MCE Cat#HY-10221, GSK-J4-
645 Selleck Cat#S7070, EPZ-6438-Selleck Cat#S7128) or 8 days (Sulfopin, generous gift from Dr.
646 Nir London's Lab, and MM-102-Selleck Cat#S7265) (Table S3). At least two replicates were
647 measured for each treatment. When treated for 8 days drug was also added at day 4. Cell
648 viability was measured by CelltiterGlo assay (G7571, Promega) according to the

649 manufacturer's instructions. Luminescence was measured by Cytation 5 plate reader and
650 viability was compared to DMSO treated control cells.

651 At least two technical replicates were averaged in each experiment, and mean ± SE of all
652 biological repeats was calculated. Two sample t-test on all technical replicates was used to
653 determine significant difference between the treatments. Bonferroni correction was applied
654 whenever more than two comparisons were made.

655 **IC50 quantification**

656 Sulfopin IC50 values were determined by 4-parameter log-logistic dose response model using
657 SynergyFinder 2.0[130].

658 **BLISS index calculation**

659 The Bliss index was calculated as the ratio between observed effect of combined drug
660 treatment and expected effect (based on the calculated effect of combining single-drug
661 treatment)[45,46]:

662 Bliss index = Observed/Expected = $\frac{J_{AB}}{(J_A \times J_B)}$

663 JA is the effect on growth of drug A only compared to DMSO

664 JB is the effect on growth of drug B only compared to DMSO

665 JAB is the effect on growth of drug A and B together compared to DMSO

666 Synergy: Bliss <1

667 Additive: Bliss=1

668 Antagonist: Blliss>1

669 **Western blot analysis**

670 An equal number of cells from different treatments were suspended in Laemmli sample buffer
671 (Bio-Rad, #1610747) containing 50mM DTT (Promega, #V3151), vortexed and heated up to
672 98°C. Samples were loaded onto Novex WedgeWell 4-20%, Tris-Glycine 4-20% gel
673 (ThermoFisher Scientific, XP04205BOX) and electrophoresis was carried out in TG-SDS
674 buffer (Bio-rad #1610732) for 1-1.5 hours at 120V. After electrophoresis, proteins were
675 transferred to nitrocellulose membranes using transfer kit (Bio-rad, #1704156), followed by
676 brief rinse in TBS (Bio-rad, #1706435) and blocking with 5% (w/v) milk powder in TBST
677 (Tween20-Sigma, #P1379) for 60 minutes. The membranes were then rinsed in TBST and
678 incubated with primary antibodies overnight at 4 °C with gentle rocking. Primary antibodies
679 (Table S1) were diluted according to manufacturer instructions in TBST containing 5% (w/v)
680 milk powder. The following day the membranes were rinsed in TBST, then incubated with

681 HRP-conjugated secondary antibody (Table S1) diluted according to manufacturer instructions
682 in a solution containing 5% (w/v) milk powder in TBST. The membranes were then rinsed in
683 TBST and dipped in an ECL WB Detection Reagent (Bio-rad #1705061) prior to exposure.
684 Membranes were imaged using a Bio-Rad ChemiDoc MP imaging system.

685 **Nucleosome preparation for single-molecule imaging**

686 Nucleosomes for single-molecule imaging were extracted and labeled as described in Furth et
687 al[16]. Briefly, 2–2.5 million cells were collected, washed once with PBS supplemented with
688 protease inhibitors cocktail, 1:100, Sigma P8340), and HDAC inhibitors (20mM Sodium
689 butyrate, Sigma 303410 and 0.1mM Vorinostat V-8477), and then resuspended in 0.05%
690 IGEPAL (Sigma I8896) diluted in PBS (supplemented with inhibitors). Cell pellets were then
691 lysed in parallel to chromatin digestion (100mM Tris-HCl pH 7.5, 300mM NaCl, 2% Triton®
692 X-100, 0.2% sodium deoxycholate, 10mM CaCl2) supplemented with inhibitors and
693 Micrococcal Nuclease (ThermoFisher Scientific, 88216). The suspension was incubated at
694 37°C for 10 min and the MNase reaction was inactivated by addition of EGTA at a final
695 concentration of 20mM. Lysate was clear by centrifugation and nucleosomes were concentrated
696 using an Amicon ultra-4 (Millipore, UFC810024). Inhibitors were supplemented following
697 concentration. Nucleosomes labeling the following reaction was used: NEBuffer™ 2 (NEB
698 B7202), inhibitors (as detailed above, 0.25 mM MnCl2, 33uM fluorescently labeled dATP
699 (Jena Bioscience, NU-1611-Cy3), 33uM biotinylated dUTP (Jena Bioscience, NU-803-BIOX),
700 1.5ul of Klenow Fragment (3'→5′ exo-, NEB, M0212S) and 1.5ul of T4 Polynucleotide Kinase
701 (NEB, M0201L). Samples were incubated at 37°C for 1h and then inactivated by addition of
702 EDTA at a final concentration of 20mM. Nucleosomes were then purified on Performa Spin
703 Columns (EdgeBio, 13266) followed by the addition of inhibitors.

704 **Surface preparation for single-molecule imaging**

705 PEG-biotin microscope slides were prepared as described in Furth et al[16]. Ibidi glass coverslips
706 (25mm×75mm, IBIDI, IBD-10812) were cleaned with (1) ddH2O (3X washes, 5 min
707 sonication, 3X washes), (2) 2% Alconox (Sigma 242985, 20min sonication followed by 5X
708 washes with ddH2O), (3) 100% Acetone (20min sonication followed by 3X washes with
709 ddH2O). Slides were then incubated in 1M KOH solution for 30min while sonicated (Sigma
710 484016), followed by 3X washes with ddH2O. Slides were sonicated for 10 min in 100% HPLC
711 EtOH (J.T baker 8462-25) and then incubated for 24 min in a mixture of 3% 3-
712 Aminopropyltriethoxysilane (ACROS Organics, 430941000) and 5% acetic acid in HPLC
713 EtOH, with 1 min sonication in the middle. Following washes with HPLC EtOH (3X) and
714 ddH2O (3X) slides were dried and mPEG:biotin-PEG solution was applied (20mg Biotin-PEG
715 (Laysan, Biotin-PEG-SVA-5000), 180mg mPEG (Laysan, MPEG-SVA-5000) dissolved in

716 1560ul 0.1M Sodium Bicarbonate (Sigma, S6297) on one surface followed by the assembly of
717 another surface on top. Surfaces were incubated overnight in a dark humid environment and at
718 the following day, were washed with ddH2O and dried. MS (PEG) 4 (ThermoFisher Scientific,
719 TS-22341) was diluted in 0.1M of sodium bicarbonate to a final concentration of 11.7 mg/mL
720 and applied on the surfaces for overnight incubation in dark humid environment. Surfaces were
721 washed with ddH2O and dried.

722 **Single-molecule imaging of histone modifications**

723 PEG-biotin coated coverslips were assembled into Ibidi flowcell (Sticky Slide VI hydrophobic,
724 IBIDI, IBD-80608). Streptavidin (SIGMA, S4762) was added to a final concentration of
725 0.2mg/mL followed by an incubation of 10 min. TetraSpeck beads (used for image alignment,
726 ThermoFisher Scientific, T7279) diluted in PBS were added and incubated on surface for at
727 least 30 min. Labeled nucleosomes were incubated for 10 min in imaging buffer (10mM MES
728 pH 6.5 (Boston Bioproducts Inc, NC9904354), 60mM KCL, 0.32mM EDTA, 3mM MgCl2,
729 10% glycerol, 0.1mg/mL BSA (Sigma, A7906), 0.02% Igepal (Sigma, I8896) to allow
730 immobilization via biotin-streptavidin interactions and washed with imaging buffer. H3K27ac
731 antibody was diluted in imaging buffer (1:2000) and incubated for 30 min. All positions (80–
732 100 fields-of-view (FOV) per experiment) were then imaged by a total internal reflection
733 (TIRF) microscope by Nikon (Ti2 LU-N4 TIRF) every 10 min (10–15 cycles).

734 Image analysis was performed with Cell Profiler image analysis tools
735 (http://www.cellprofiler.org/) as described in Furth et al[16]. Image analysis is done in two steps:
736 (1) Time-lapse images of antibody binding events and TetraSpeck beads are aligned, stacked
737 and summed to one image. Antibody spots and TetraSpeck beads spots were distinguished
738 based on the size of the spot. (2) Stacked images are aligned to the initial images of the
739 nucleosomes based on TetraSpeck beads location spots, and only binding events that align with
740 nucleosomes are filtered and saved for further analysis. To evaluate random co-localization
741 (negative control), each stacked image is aligned to a 90° flipped image of the initial
742 nucleosomes. The use of TetraSpeck beads and a highly accurate microscope stage allowed
743 alignment of images with shifts of up to 30 pixels. Nucleosomes are initially distributed on the
744 surface in low density to minimize overlap between spots. Average percentage of modified
745 nucleosomes over all fields of view (FOV) imaged was calculated in each experiment. Mean ±
746 SE of three to five biological repeats was calculated. Two sample t-test on all biological repeats
747 was used to determine significant difference between the treatments.

748 **Mouse injection and treatment**

749 All animal experiments were conducted in accordance with approved institutional animal care
750 and use committee protocols. Mice were housed and handled in a specific-pathogen-free,

751 temperature-controlled (22°C ± 1°C) mouse facility on a reverse 12/12 h light/dark cycle,
752 Animals were fed a regular chow diet et libitum. Single-cell suspension of SU-DIPG13P* or
753 SU-DIPG13 cells were stereotactically injected into the pons of male NGS mice (NOD-SCID-
754 IL2R gamma chain-deficient, The Jackson Laboratory) as previously described in Venkatesh
755 et al[104]. Injection coordinates were: 0.8 mm posterior to lambda, 1 mm lateral to the sagittal
756 suture, and 5 mm deep. Briefly, the skull of the mouse was exposed, and a small bore hole (0.5
757 mm) was made using a high-speed drill at the appropriate stereotactic coordinates.
758 Approximately 300,000-400,000 cells in 3ul volume were injected at a speed of 0.3ul per
759 minute into the pons with a 26-gauge Hamilton syringe; following 10 min pause, the needle
760 was removed at a speed of 0.2 mm/minute. After closing the scalp, mice were placed on a
761 heating pad and returned to their cages after full recovery. Mice were randomized to treatment
762 groups, and treatment started 10 days (SU-DIPG13P*) or 5 weeks (SU-DIPG13) post-injection.
763 Treatment was given daily for 18 days, by intraperitoneal injection according to the following
764 groups: Vorinostat 200mg/kg daily (LC, V-8477-SU-DIPG13P*; MCE, HY-10221- SU-
765 DIPG13), Sulfopin 40 mg/kg (gift from Dr. Nir London's Lab), combination 200 mg/kg
766 Vorinostst and 40 mg/kg Sulfopin, control mice received solvent 15% DMSO in 50% PEG400
767 (Sigma) in 0.15M NaCl.

768 **Tumor size imaging using IVIS**

769 For bioluminescence imaging, mice received 100 µl D-luciferin (33 mg/ml; Perkin-elmer,
770 Cat#122799) intraperitoneally 10 min before isoflurane anesthesia and were placed in LagoX
771 Imaging System (Spectral Instruments Imaging).

772 The bioluminescence signal was measured using the ROI tool in LagoX software (Spectral
773 Instruments Imaging). The fold change in total Photon flux (p/s) over time was used to compare
774 tumor growth between the groups. Mann-Whitney U-test (Two-tailed) was used to determine
775 significant difference between the DMSO and Sulfopin+Vorinostat treated mice.

776 **Mouse brain slides staining**

777 Brains were collected, fixed in 4% paraformaldehyde, and embedded in paraffin blocks. For
778 H3-K27M and mTOR staining, slides were de-paraffinized (1-Xylene –Bio-lab #242500; 2-
779 Xylene; 3-Eth 100%-Bio-lab #05250501;4- Eth- 96%; 5-Eth-70%;) and incubated in acetone
780 (Bio-lab, #010352) at -20C. Slides were incubated in hydrogen peroxide blocking solution
781 (200ml Methanol-Bio-lab #136805, 1% HCl-Bio-lab #084102, 3% H2O2- JT Baker #2186-01)
782 for blocking endogenous peroxidase activity. Antigen retrieval was performed using citric acid
783 buffer at pH-6, followed by blocking with 20% NHS and 0.5% triton in PBS. Rabbit anti mTOR
784 (1:100, Table S1) was diluted in 2% NHS and 0.5% triton and was incubated overnight at room
785 temperature. Slides were then incubated with HRP conjugated goat anti rabbit (1:100, Table

786 S1) diluted 2% NHS for 1.5hr followed by OPAL 650 (1:500, Akoya FP1496001KT) reagent
787 incubation for 15 min. Antibodies were stripped using microwave treatment with citric acid at
788 pH-6, blocked and again incubated with rabbit anti H3-K27M (1:100 table S1) overnight at
789 room temperature. Slides were then incubated with HRP conjugated goat anti rabbit (1:100,
790 Table S1) diluted 2% NHS for 1.5hr followed by OPAL 570 (1:500, Akoya FP1488001KT)
791 reagent incubation for 15 min. Slides were then washed with PBS and incubated with Hoechst
792 (1:1000) for 1 minutes, followed by mounting with 25x75x1mm glass slides using Aqua-
793 Poly/Mount Mounting Medium. All slides were scanned using the Panoramic MIDI slide
794 scanner (3D Histech, Hungary) at x20 magnification, to receive a full scan of the tumor section.

795 For H3-K27M and mTOR co-localization analysis, double stained cells were counted using
796 ImageJ. First, threshold based segmentation was used to detect positive cells in each of the
797 channels and the image calculator feature was used to find the double positive cells. The total
798 number of double-positive cells was then divided by to total number of H3-K27M-positive cells
799 to calculate the percentage co-localization\H3-K27M cells. Similar-sized FOVs were used for
800 all the images analyzed, and 13-198 H3-K27M-positive cells were detected per FOV (an
801 average of 90 cells per FOV). For mTOR signal quantification in non-tumor cells (mice cells)
802 a region of interest was selected in a location on the section with no positive H3-K27M cells.
803 Threshold based segmentation was used to detect the percentage mTOR stained area.

804 **Statistical analysis**

805 Unless noted otherwise, p values were determined using two-sample t-test and are indicated in
806 the figure legends.

807 Pearson correlation coefficient was used to assess the relationship between all variables. Scatter
808 plot was generated using ggscatter (R ggpubr package).

809

810 **References**

811 1. Johung, T.B., and Monje, M. (2016). Diffuse Intrinsic Pontine Glioma: New
812 Pathophysiological Insights and Emerging Therapeutic Targets. Curr Neuropharmacol
813 *15*. 10.2174/1570159x14666160509123229.

814 2. Hayden, E., Holliday, H., Lehmann, R., Khan, A., Tsoli, M., Rayner, B.S., and
815 Ziegler, D.S. (2021). Therapeutic targets in diffuse midline gliomas—an emerging
816 landscape. Cancers (Basel) *13*. 10.3390/cancers13246251.

817 3. Ostrom, Q.T., Gittleman, H., Fulop, J., Liu, M., Blanda, R., Kromer, C., Wolinsky, Y.,
818 Kruchko, C., and Barnholtz-Sloan, J.S. (2015). CBTRUS statistical Report: primary
819 brain and central nervous system tumors diagnosed in the United States in 2008-2012.
820 Neuro Oncol *17*. 10.1093/neuonc/nov189.

821 4. Srikanthan, D., Taccone, M.S., Van Ommeren, R., Ishida, J., Krumholtz, S.L., and
822 Rutka, J.T. (2021). Diffuse intrinsic pontine glioma: current insights and future
823 directions. Chin Neurosurg J *7*. 10.1186/s41016-020-00218-w.

824 5. Castel, D., Philippe, C., Calmon, R., Le Dret, L., Truffaux, N., Boddaert, N., Pagès,
825 M., Taylor, K.R., Saulnier, P., Lacroix, L., et al. (2015). Histone H3F3A and
826 HIST1H3B K27M mutations define two subgroups of diffuse intrinsic pontine gliomas
827 with different prognosis and phenotypes. Acta Neuropathol *130*. 10.1007/s00401-015-
828 1478-0.

829 6. Fontebasso, A.M., Papillon-Cavanagh, S., Schwartzentruber, J., Nikbakht, H., Gerges,
830 N., Fiset, P.O., Bechet, D., Faury, D., De Jay, N., Ramkissoon, L.A., et al. (2014).
831 Recurrent somatic mutations in ACVR1 in pediatric midline high-grade astrocytoma.
832 Nat Genet *46*. 10.1038/ng.2950.

833 7. Schwartzentruber, J., Korshunov, A., Liu, X.Y., Jones, D.T.W., Pfaff, E., Jacob, K.,
834 Sturm, D., Fontebasso, A.M., Quang, D.A.K., Tönjes, M., et al. (2012). Erratum:
835 Driver mutations in histone H3.3 and chromatin remodelling genes in paediatric
836 glioblastoma (Nature (2012) 482 (226-231)). Nature *484*. 10.1038/nature11026.

837 8. Wu, G., Broniscer, A., McEachron, T.A., Lu, C., Paugh, B.S., Becksfort, J., Qu, C.,
838 Ding, L., Huether, R., Parker, M., et al. (2012). Somatic histone H3 alterations in
839 pediatric diffuse intrinsic pontine gliomas and non-brainstem glioblastomas. Nat Genet
840 *44*. 10.1038/ng.1102.

841 9. Bender, S., Tang, Y., Lindroth, A.M., Hovestadt, V., Jones, D.T.W., Kool, M.,
842 Zapatka, M., Northcott, P.A., Sturm, D., Wang, W., et al. (2013). Reduced H3K27me3

843 and DNA Hypomethylation Are Major Drivers of Gene Expression in K27M Mutant
844 Pediatric High-Grade Gliomas. Cancer Cell *24*. 10.1016/j.ccr.2013.10.006.

845 10. Chan, K.M., Fang, D., Gan, H., Hashizume, R., Yu, C., Schroeder, M., Gupta, N.,
846 Mueller, S., David James, C., Jenkins, R., et al. (2013). The histone H3.3K27M
847 mutation in pediatric glioma reprograms H3K27 methylation and gene expression.
848 Genes Dev *27*. 10.1101/gad.217778.113.

849 11. Lewis, P.W., Müller, M.M., Koletsky, M.S., Cordero, F., Lin, S., Banaszynski, L.A.,
850 Garcia, B.A., Muir, T.W., Becher, O.J., and Allis, C.D. (2013). Inhibition of PRC2
851 activity by a gain-of-function H3 mutation found in pediatric glioblastoma. Science
852 (1979) *340*. 10.1126/science.1232245.

853 12. Krug, B., De Jay, N., Harutyunyan, A.S., Deshmukh, S., Marchione, D.M.,
854 Guilhamon, P., Bertrand, K.C., Mikael, L.G., McConechy, M.K., Chen, C.C.L., et al.
855 (2019). Pervasive H3K27 Acetylation Leads to ERV Expression and a Therapeutic
856 Vulnerability in H3K27M Gliomas. Cancer Cell *35*. 10.1016/j.ccell.2019.04.004.

857 13. Piunti, A., Hashizume, R., Morgan, M.A., Bartom, E.T., Horbinski, C.M., Marshall,
858 S.A., Rendleman, E.J., Ma, Q., Takahashi, Y.H., Woodfin, A.R., et al. (2017).
859 Therapeutic targeting of polycomb and BET bromodomain proteins in diffuse intrinsic
860 pontine gliomas. Nat Med *23*. 10.1038/nm.4296.

861 14. Harpaz, N., Mittelman, T., Beresh, O., Griess, O., Furth, N., Salame, T.M., Oren, R.,
862 Fellus-Alyagor, L., Harmelin, A., Alexandrescu, S., et al. (2022). Single-cell
863 epigenetic analysis reveals principles of chromatin states in H3.3-K27M gliomas. Mol
864 Cell *82*, 2696-2713.e9. 10.1016/j.molcel.2022.05.023.

865 15. Filbin, M., and Monje, M. (2019). Developmental origins and emerging therapeutic
866 opportunities for childhood cancer. Nat Med *25*. 10.1038/s41591-019-0383-9.

867 16. Furth, N., Algranati, D., Dassa, B., Beresh, O., Fedyuk, V., Morris, N., Kasper, L.H.,
868 Jones, D., Monje, M., Baker, S.J., et al. (2022). H3-K27M-mutant nucleosomes
869 interact with MLL1 to shape the glioma epigenetic landscape. Cell Rep *39*.
870 10.1016/j.celrep.2022.110836.

871 17. Grasso, C.S., Tang, Y., Truffaux, N., Berlow, N.E., Liu, L., Debily, M.A., Quist, M.J.,
872 Davis, L.E., Huang, E.C., Woo, P.J., et al. (2015). Functionally defined therapeutic
873 targets in diffuse intrinsic pontine glioma. Nat Med *21*. 10.1038/nm.3855.

874 18. Yin, D., Ong, J.M., Hu, J., Desmond, J.C., Kawamata, N., Konda, B.M., Black, K.L.,
875 and Koeffler, H.P. (2007). Suberoylanilide hydroxamic acid, a histone deacetylase

876 inhibitor: Effects on gene expression and growth of glioma cells in vitro and in vivo.
877 Clinical Cancer Research *13*. 10.1158/1078-0432.CCR-06-1261.

878 19. Su, J.M., Kilburn, L.B., Mansur, D.B., Krailo, M., Buxton, A., Adekunle, A., Gajjar,
879 A., Adamson, P.C., Weigel, B., Fox, E., et al. (2022). Phase I/II trial of vorinostat and
880 radiation and maintenance vorinostat in children with diffuse intrinsic pontine glioma:
881 A Children's Oncology Group report. Neuro Oncol *24*. 10.1093/neuonc/noab188.

882 20. Chen, H., Liu, H., and Qing, G. (2018). Targeting oncogenic Myc as a strategy for
883 cancer treatment. Signal Transduct Target Ther *3*. 10.1038/s41392-018-0008-7.

884 21. Buczkowicz, P., Hoeman, C., Rakopoulos, P., Pajovic, S., Letourneau, L., Dzamba,
885 M., Morrison, A., Lewis, P., Bouffet, E., Bartels, U., et al. (2014). Genomic analysis of
886 diffuse intrinsic pontine gliomas identifies three molecular subgroups and recurrent
887 activating ACVR1 mutations. Nat Genet *46*. 10.1038/ng.2936.

888 22. Mackay, A., Burford, A., Carvalho, D., Izquierdo, E., Fazal-Salom, J., Taylor, K.R.,
889 Bjerke, L., Clarke, M., Vinci, M., Nandhabalan, M., et al. (2017). Integrated Molecular
890 Meta-Analysis of 1,000 Pediatric High-Grade and Diffuse Intrinsic Pontine Glioma.
891 Cancer Cell *32*. 10.1016/j.ccell.2017.08.017.

892 23. Pajovic, S., Siddaway, R., Bridge, T., Sheth, J., Rakopoulos, P., Kim, B., Ryall, S.,
893 Agnihotri, S., Phillips, L., Yu, M., et al. (2020). Epigenetic activation of a RAS/MYC
894 axis in H3.3K27M-driven cancer. Nat Commun *11*. 10.1038/s41467-020-19972-7.

895 24. Dubois, F.P.B., Shapira, O., Greenwald, N.F., Zack, T., Wala, J., Tsai, J.W., Crane, A.,
896 Baguette, A., Hadjadj, D., Harutyunyan, A.S., et al. (2022). Structural variants shape
897 driver combinations and outcomes in pediatric high-grade glioma. Nat Cancer *3*, 994–
898 1011. 10.1038/s43018-022-00403-z.

899 25. Wang, C., Zhang, J., Yin, J., Gan, Y., Xu, S., Gu, Y., and Huang, W. (2021).
900 Alternative approaches to target Myc for cancer treatment. Signal Transduct Target
901 Ther *6*. 10.1038/s41392-021-00500-y.

902 26. Dubiella, C., Pinch, B.J., Koikawa, K., Zaidman, D., Poon, E., Manz, T.D., Nabet, B.,
903 He, S., Resnick, E., Rogel, A., et al. (2021). Sulfopin is a covalent inhibitor of Pin1
904 that blocks Myc-driven tumors in vivo. Nat Chem Biol *17*. 10.1038/s41589-021-
905 00786-7.

906 27. Farrell, A.S., Pelz, C., Wang, X., Daniel, C.J., Wang, Z., Su, Y., Janghorban, M.,
907 Zhang, X., Morgan, C., Impey, S., et al. (2013). Pin1 Regulates the Dynamics of c-
908 Myc DNA Binding To Facilitate Target Gene Regulation and Oncogenesis. Mol Cell
909 Biol *33*. 10.1128/mcb.01455-12.

910 28. D'Artista, L., Bisso, A., Piontini, A., Doni, M., Verrecchia, A., Kress, T.R., Morelli,
911 M.J., Del Sal, G., Amati, B., and Campaner, S. (2016). Pin1 is required for sustained B
912 cell proliferation upon oncogenic activation of Myc. Oncotarget *7*.
913 10.18632/oncotarget.7846.

914 29. Hölzel, M., Rohrmoser, M., Schlee, M., Grimm, T., Harasim, T., Malamoussi, A.,
915 Gruber-Eber, A., Kremmer, E., Hiddemann, W., Bornkamm, G.W., et al. (2005).
916 Mammalian WDR12 is a novel member of the Pes1-Bop1 complex and is required for
917 ribosome biogenesis and cell proliferation. Journal of Cell Biology *170*.
918 10.1083/jcb.200501141.

919 30. Teng, S.C., Chen, Y.Y., Su, Y.N., Chou, P.C., Chiang, Y.C., Tseng, S.F., and Wu, K.J.
920 (2004). Direct Activation of HSP90A Transcription by c-Myc Contributes to c-Myc-
921 induced Transformation. Journal of Biological Chemistry *279*.
922 10.1074/jbc.M308842200.

923 31. Skene, P.J., and Henikoff, S. (2017). An efficient targeted nuclease strategy for high-
924 resolution mapping of DNA binding sites. Elife *6*. 10.7554/eLife.21856.

925 32. Ferrari, K.J., Scelfo, A., Jammula, S.G., Cuomo, A., Barozzi, I., Stützer, A., Fischle,
926 W., Bonaldi, T., and Pasini, D. (2014). Polycomb-Dependent H3K27me1 and
927 H3K27me2 Regulate Active Transcription and Enhancer Fidelity. Mol Cell *53*.
928 10.1016/j.molcel.2013.10.030.

929 33. Mohammad, F., Weissmann, S., Leblanc, B., Pandey, D.P., Højfeldt, J.W., Comet, I.,
930 Zheng, C., Johansen, J.V., Rapin, N., Porse, B.T., et al. (2017). EZH2 is a potential
931 therapeutic target for H3K27M-mutant pediatric gliomas. Nat Med *23*.
932 10.1038/nm.4293.

933 34. Jain, S.U., Rashoff, A.Q., Krabbenhoft, S.D., Hoelper, D., Do, T.J., Gibson, T.J.,
934 Lundgren, S.M., Bondra, E.R., Deshmukh, S., Harutyunyan, A.S., et al. (2020). H3
935 K27M and EZHIP Impede H3K27-Methylation Spreading by Inhibiting Allosterically
936 Stimulated PRC2. Mol Cell *80*. 10.1016/j.molcel.2020.09.028.

937 35. Berlow, N.E., Svalina, M.N., Quist, M.J., Settelmeyer, T.P., Zherebitskiy, V., Kogiso,
938 M., Qi, L., Du, Y., Hawkins, C.E., Hulleman, E., et al. (2018). IL-13 receptors as
939 possible therapeutic targets in diffuse intrinsic pontine glioma. PLoS One *13*.
940 10.1371/journal.pone.0193565.

941 36. Yeh, E.S., and Means, A.R. (2007). PIN1, the cell cycle and cancer. Nat Rev Cancer *7*.
942 10.1038/nrc2107.

943 37. Pinch, B.J., Doctor, Z.M., Nabet, B., Browne, C.M., Seo, H.S., Mohardt, M.L.,
944 Kozono, S., Lian, X., Manz, T.D., Chun, Y., et al. (2020). Identification of a potent
945 and selective covalent Pin1 inhibitor. Nat Chem Biol *16*. 10.1038/s41589-020-0550-9.

946 38. Lin, G.L., Wilson, K.M., Ceribelli, M., Stanton, B.Z., Woo, P.J., Kreimer, S., Qin,
947 E.Y., Zhang, X., Lennon, J., Nagaraja, S., et al. (2019). Therapeutic strategies for
948 diffuse midline glioma from high-throughput combination drug screening. Sci Transl
949 Med *11*. 10.1126/scitranslmed.aaw0064.

950 39. Harutyunyan, A.S., Krug, B., Chen, H., Papillon-Cavanagh, S., Zeinieh, M., De Jay,
951 N., Deshmukh, S., Chen, C.C.L., Belle, J., Mikael, L.G., et al. (2019). H3K27M
952 induces defective chromatin spread of PRC2-mediated repressive H3K27me2/me3 and
953 is essential for glioma tumorigenesis. Nat Commun *10*. 10.1038/s41467-019-09140-x.

954 40. Schuettengruber, B., Bourbon, H.M., Di Croce, L., and Cavalli, G. (2017). Genome
955 Regulation by Polycomb and Trithorax: 70 Years and Counting. Cell *171*.
956 10.1016/j.cell.2017.08.002.

957 41. Stafford, J.M., Lee, C.H., Voigt, P., Descostes, N., Saldana-Meyer, R., Yu, J.R.,
958 Leroy, G., Oksuz, O., Chapman, J.R., Suarez, F., et al. (2018). Multiple modes of
959 PRC2 inhibition elicit global chromatin alterations in H3K27M pediatric glioma. Sci
960 Adv *4*. 10.1126/sciadv.aau5935.

961 42. Jain, S.U., Do, T.J., Lund, P.J., Rashoff, A.Q., Diehl, K.L., Cieslik, M., Bajic, A.,
962 Juretic, N., Deshmukh, S., Venneti, S., et al. (2019). PFA ependymoma-associated
963 protein EZHIP inhibits PRC2 activity through a H3 K27M-like mechanism. Nat
964 Commun *10*. 10.1038/s41467-019-09981-6.

965 43. Agger, K., Cloos, P.A.C., Christensen, J., Pasini, D., Rose, S., Rappsilber, J., Issaeva,
966 I., Canaani, E., Salcini, A.E., and Helin, K. (2007). UTX and JMJD3 are histone
967 H3K27 demethylases involved in HOX gene regulation and development. Nature *449*.
968 10.1038/nature06145.

969 44. Hashizume, R., Andor, N., Ihara, Y., Lerner, R., Gan, H., Chen, X., Fang, D., Huang,
970 X., Tom, M.W., Ngo, V., et al. (2014). Pharmacologic inhibition of histone
971 demethylation as a therapy for pediatric brainstem glioma. Nat Med *20*.
972 10.1038/nm.3716.

973 45. Yadav, B., Wennerberg, K., Aittokallio, T., and Tang, J. (2015). Searching for Drug
974 Synergy in Complex Dose-Response Landscapes Using an Interaction Potency Model.
975 Comput Struct Biotechnol J *13*. 10.1016/j.csbj.2015.09.001.

976 46. BLISS, C.I. (1939). THE TOXICITY OF POISONS APPLIED JOINTLY. Annals of
977 Applied Biology *26*. 10.1111/j.1744-7348.1939.tb06990.x.

978 47. Nagaraja, S., Quezada, M.A., Gillespie, S.M., Arzt, M., Lennon, J.J., Woo, P.J.,
979 Hovestadt, V., Kambhampati, M., Filbin, M.G., Suva, M.L., et al. (2019). Histone
980 Variant and Cell Context Determine H3K27M Reprogramming of the Enhancer
981 Landscape and Oncogenic State. Mol Cell *76*. 10.1016/j.molcel.2019.08.030.

982 48. Jessa, S., Mohammadnia, A., Harutyunyan, A.S., Hulswit, M., Varadharajan, S.,
983 Lakkis, H., Kabir, N., Bashardanesh, Z., Hébert, S., Faury, D., et al. (2022). K27M in
984 canonical and noncanonical H3 variants occurs in distinct oligodendroglial cell
985 lineages in brain midline gliomas. Nat Genet *54*. 10.1038/s41588-022-01205-w.

986 49. Annovazzi, L., Mellai, M., Caldera, V., Valente, G., Tessitore, L., and Schiffer, D.
987 (2009). mTOR, S6 and AKT expression in relation to proliferation and
988 apoptosis/autophagy in glioma. Anticancer Res *29*.

989 50. Ma, S., Pang, C., Song, L., Guo, F., and Sun, H. (2015). Activating transcription factor
990 3 is overexpressed in human glioma and its knockdown in glioblastoma cells causes
991 growth inhibition both in vitro and in vivo. Int J Mol Med *35*.
992 10.3892/ijmm.2015.2173.

993 51. Xue, H., Zhang, J., Guo, X., Wang, J., Li, J., Gao, X., Guo, X., Li, T., Xu, S., Zhang,
994 P., et al. (2016). CREBRF is a potent tumor suppressor of glioblastoma by blocking
995 hypoxia-induced autophagy via the CREB3/ATG5 pathway. Int J Oncol *49*.
996 10.3892/ijo.2016.3576.

997 52. Tang, P., Steck, P.A., and Yung, W.K.A. (1997). The autocrine loop of TGF-α/EGFR
998 and brain tumors. J Neurooncol *35*. 10.1023/A:1005824802617.

999 53. Abdouh, M., Facchino, S., Chatoo, W., Balasingam, V., Ferreira, J., and Bernier, G.
1000 (2009). BMI1 sustains human glioblastoma multiforme stem cell renewal. Journal of
1001 Neuroscience *29*. 10.1523/JNEUROSCI.0968-09.2009.

1002 54. Zhang, H., Kong, Q., Wang, J., Jiang, Y., and Hua, H. (2020). Complex roles of
1003 cAMP–PKA–CREB signaling in cancer. Exp Hematol Oncol *9*. 10.1186/s40164-020-
1004 00191-1.

1005 55. West, A.J., Tsui, V., Stylli, S.S., Nguyen, H.P.T., Morokoff, A.P., Kaye, A.H., and
1006 Luwor, R.B. (2018). The role of interleukin-6-STAT3 signalling in glioblastoma.
1007 Oncol Lett *16*. 10.3892/ol.2018.9227.

1008 56. Kennedy, B.K., and Lamming, D.W. (2016). The Mechanistic Target of Rapamycin:
1009 The Grand ConducTOR of Metabolism and Aging. Cell Metab *23*.
1010 10.1016/j.cmet.2016.05.009.

1011 57. Shamloo, B., and Usluer, S. (2019). P21 in cancer research. Cancers (Basel) *11*.
1012 10.3390/cancers11081178.

1013 58. Tahmasebi, S., Alain, T., Rajasekhar, V.K., Zhang, J.P., Prager-Khoutorsky, M.,
1014 Khoutorsky, A., Dogan, Y., Gkogkas, C.G., Petroulakis, E., Sylvestre, A., et al.
1015 (2014). Multifaceted regulation of somatic cell reprogramming by mRNA translational
1016 control. Cell Stem Cell *14*. 10.1016/j.stem.2014.02.005.

1017 59. Cui, D., Qu, R., Liu, D., Xiong, X., Liang, T., and Zhao, Y. (2021). The Cross Talk
1018 Between p53 and mTOR Pathways in Response to Physiological and Genotoxic
1019 Stresses. Front Cell Dev Biol *9*. 10.3389/fcell.2021.775507.

1020 60. Minucci, S., and Pelicci, P.G. (2006). Histone deacetylase inhibitors and the promise
1021 of epigenetic (and more) treatments for cancer. Nat Rev Cancer *6*. 10.1038/nrc1779.

1022 61. Poole, C.J., and van Riggelen, J. (2017). MYC—master regulator of the cancer
1023 epigenome and transcriptome. Genes (Basel) *8*. 10.3390/genes8050142.

1024 62. Kanai, Y. (2022). Amino acid transporter LAT1 (SLC7A5) as a molecular target for
1025 cancer diagnosis and therapeutics. Pharmacol Ther *230*.
1026 10.1016/j.pharmthera.2021.107964.

1027 63. Lee, D.W., Ramakrishnan, D., Valenta, J., Parney, I.F., Bayless, K.J., and Sitcheran,
1028 R. (2013). The NF-κB RelB Protein Is an Oncogenic Driver of Mesenchymal Glioma.
1029 PLoS One *8*. 10.1371/journal.pone.0057489.

1030 64. Feng, Y., Lei, X., Zhang, L., Wan, H., Pan, H., Wu, J., Zou, M., Zhu, L., and Mi, Y.
1031 (2021). COPB2: a transport protein with multifaceted roles in cancer development and
1032 progression. Clinical and Translational Oncology *23*. 10.1007/s12094-021-02630-9.

1033 65. Zhou, D., Tang, W., Su, G., Cai, M., An, H.X., and Zhang, Y. (2017). PCDH18 is
1034 frequently inactivated by promoter methylation in colorectal cancer. Sci Rep *7*.
1035 10.1038/s41598-017-03133-w.

1036 66. Fernández-Medarde, A., and Santos, E. (2011). Ras in cancer and developmental
1037 diseases. Genes Cancer *2*. 10.1177/1947601911411084.

1038 67. Braicu, C., Buse, M., Busuioc, C., Drula, R., Gulei, D., Raduly, L., Rusu, A., Irimie,
1039 A., Atanasov, A.G., Slaby, O., et al. (2019). A comprehensive review on MAPK: A
1040 promising therapeutic target in cancer. Cancers (Basel) *11*. 10.3390/cancers11101618.

1041 68. Rascio, F., Spadaccino, F., Rocchetti, M.T., Castellano, G., Stallone, G., Netti, G.S.,
1042 and Ranieri, E. (2021). The pathogenic role of PI3K/AKT pathway in cancer onset and
1043 drug resistance: an updated review. Cancers (Basel) *13*. 10.3390/cancers13163949.

1044 69. Peng, Y., Wang, Y., Zhou, C., Mei, W., and Zeng, C. (2022). PI3K/Akt/mTOR
1045 Pathway and Its Role in Cancer Therapeutics: Are We Making Headway? Front Oncol
1046 *12*. 10.3389/fonc.2022.819128.

1047 70. Mure, H., Matsuzaki, K., Kitazato, K.T., Mizobuchi, Y., Kuwayama, K., Kageji, T.,
1048 and Nagahiro, S. (2010). Akt2 and Akt3 play a pivotal role in malignant gliomas.
1049 Neuro Oncol *12*. 10.1093/neuonc/nop026.

1050 71. Ding, Z., Kloss, J.M., Tuncali, S., Tran, N.L., and Loftus, J.C. (2020). TROY signals
1051 through JAK1-STAT3 to promote glioblastoma cell migration and resistance.
1052 Neoplasia (United States) *22*. 10.1016/j.neo.2020.06.005.

1053 72. Tu, Y., Zhong, Y., Fu, J., Cao, Y., Fu, G., Tian, X., and Wang, B. (2011). Activation
1054 of JAK/STAT signal pathway predicts poor prognosis of patients with gliomas.
1055 Medical Oncology *28*. 10.1007/s12032-010-9435-1.

1056 73. Raychaudhuri, B., Han, Y., Lu, T., and Vogelbaum, M.A. (2007). Aberrant
1057 constitutive activation of nuclear factor κB in glioblastoma multiforme drives invasive
1058 phenotype. J Neurooncol *85*. 10.1007/s11060-007-9390-7.

1059 74. Bar-Peled, L., Chantranupong, L., Cherniack, A.D., Chen, W.W., Ottina, K.A.,
1060 Grabiner, B.C., Spear, E.D., Carter, S.L., Meyerson, M., and Sabatini, D.M. (2013). A
1061 tumor suppressor complex with GAP activity for the Rag GTPases that signal amino
1062 acid sufficiency to mTORC1. Science (1979) *340*. 10.1126/science.1232044.

1063 75. Cai, W., Wei, Y., Jarnik, M., Reich, J., and Lilly, M.A. (2016). The GATOR2
1064 Component Wdr24 Regulates TORC1 Activity and Lysosome Function. PLoS Genet
1065 *12*. 10.1371/journal.pgen.1006036.

1066 76. Langenkamp, E., Zhang, L., Lugano, R., Huang, H., Elhassan, T.E.A., Georganaki,
1067 M., Bazzar, W., Lööf, J., Trendelenburg, G., Essand, M., et al. (2015). Elevated
1068 expression of the C-Type Lectin CD93 in the glioblastoma vasculature regulates
1069 cytoskeletal rearrangements that enhance vessel function and reduce host survival.
1070 Cancer Res *75*. 10.1158/0008-5472.CAN-14-3636.

1071 77. Sharma, S. V., Lee, D.Y., Li, B., Quinlan, M.P., Takahashi, F., Maheswaran, S.,
1072 McDermott, U., Azizian, N., Zou, L., Fischbach, M.A., et al. (2010). A Chromatin-
1073 Mediated Reversible Drug-Tolerant State in Cancer Cell Subpopulations. Cell *141*.
1074 10.1016/j.cell.2010.02.027.

1075 78. Knoechel, B., Roderick, J.E., Williamson, K.E., Zhu, J., Lohr, J.G., Cotton, M.J.,
1076 Gillespie, S.M., Fernandez, D., Ku, M., Wang, H., et al. (2014). An epigenetic
1077 mechanism of resistance to targeted therapy in T cell acute lymphoblastic leukemia.
1078 Nat Genet *46*. 10.1038/ng.2913.

1079 79. Nagaraja, S., Vitanza, N.A., Woo, P.J., Taylor, K.R., Liu, F., Zhang, L., Li, M., Meng,
1080 W., Ponnuswami, A., Sun, W., et al. (2017). Transcriptional Dependencies in Diffuse
1081 Intrinsic Pontine Glioma. Cancer Cell *31*. 10.1016/j.ccell.2017.03.011.

1082 80. Cooney, T., Onar-Thomas, A., Huang, J., Lulla, R., Fangusaro, J., Kramer, K., Baxter,
1083 P., Fouladi, M., Dunkel, I.J., Warren, K.E., et al. (2018). DIPG-22. A PHASE 1
1084 TRIAL OF THE HISTONE DEACETYLASE INHIBITOR PANOBINOSTAT IN
1085 PEDIATRIC PATIENTS WITH RECURRENT OR REFRACTORY DIFFUSE
1086 INTRINSIC PONTINE GLIOMA: A PEDIATRIC BRAIN TUMOR CONSORTIUM
1087 (PBTC) STUDY. Neuro Oncol *20*. 10.1093/neuonc/noy059.115.

1088 81. Hennika, T., Hu, G., Olaciregui, N.G., Barton, K.L., Ehteda, A., Chitranjan, A.,
1089 Chang, C., Gifford, A.J., Tsoli, M., Ziegler, D.S., et al. (2017). Pre-clinical study of
1090 panobinostat in xenograft and genetically engineered murine diffuse intrinsic pontine
1091 glioma models. PLoS One *12*. 10.1371/journal.pone.0169485.

1092 82. Leszczynska, K.B., Jayaprakash, C., Kaminska, B., and Mieczkowski, J. (2021).
1093 Emerging Advances in Combinatorial Treatments of Epigenetically Altered Pediatric
1094 High-Grade H3K27M Gliomas. Front Genet *12*. 10.3389/fgene.2021.742561.

1095 83. Oster, S.K., Ho, C.S.W., Soucie, E.L., and Penn, L.Z. (2002). The myc oncogene:
1096 Marvelously complex. Adv Cancer Res *84*. 10.1016/S0065-230X(02)84004-0.

1097 84. Pelengaris, S., Khan, M., and Evan, G. (2002). c-MYC: More than just a matter of life
1098 and death. Nat Rev Cancer *2*. 10.1038/nrc904.

1099 85. Akhavan, D., Cloughesy, T.F., and Mischel, P.S. (2010). mTOR signaling in
1100 glioblastoma: Lessons learned from bench to bedside. Neuro Oncol *12*.
1101 10.1093/neuonc/noq052.

1102 86. Warren, K.E., Killian, K., Suuriniemi, M., Wang, Y., Quezado, M., and Meltzer, P.S.
1103 (2012). Genomic aberrations in pediatric diffuse intrinsic pontine gliomas. Neuro
1104 Oncol *14*. 10.1093/neuonc/nor190.

1105 87. Panditharatna, E., Yaeger, K., Kilburn, L.B., Packer, R.J., and Nazarian, J. (2015).
1106 Clinicopathology of diffuse intrinsic pontine glioma and its redefined genomic and
1107 epigenomic landscape. Cancer Genet *208*. 10.1016/j.cancergen.2015.04.008.

1108 88. Zarghooni, M., Bartels, U., Lee, E., Buczkowicz, P., Morrison, A., Huang, A., Bouffet,
1109 E., and Hawkins, C. (2010). Whole-genome profiling of pediatric diffuse intrinsic
1110 pontine gliomas highlights platelet-derived growth factor receptor α and poly (ADP-
1111 ribose) polymerase as potential therapeutic targets. Journal of Clinical Oncology *28*.
1112 10.1200/JCO.2009.25.5463.

1113 89. Tsoli, M., Liu, J., Franshaw, L., Shen, H., Cheng, C., Jung, M.S., Joshi, S., Ehteda, A.,
1114 Khan, A., Montero-Carcabosso, A., et al. (2018). Dual targeting of mitochondrial
1115 function and mTOR pathway as a therapeutic strategy for diffuse intrinsic pontine
1116 glioma. Oncotarget *9*. 10.18632/oncotarget.24045.

1117 90. Guertin, D.A., and Sabatini, D.M. (2009). The pharmacology of mTOR inhibition. Sci
1118 Signal *2*. 10.1126/scisignal.267pe24.

1119 91. Zoncu, R., Efeyan, A., and Sabatini, D.M. (2011). MTOR: From growth signal
1120 integration to cancer, diabetes and ageing. Nat Rev Mol Cell Biol *12*.
1121 10.1038/nrm3025.

1122 92. Schmidt, E. V., Ravitz, M.J., Chen, L., and Lynch, M. (2009). Growth controls
1123 connect: Interactions between c-myc and the tuberous sclerosis complex-mTOR
1124 pathway. Cell Cycle *8*. 10.4161/cc.8.9.8215.

1125 93. Sodi, V.L., Khaku, S., Krutilina, R., Schwab, L.P., Vocadlo, D.J., Seagroves, T.N., and
1126 Reginato, M.J. (2015). MTOR/MYCAxis regulates O-GlcNAc transferase expression
1127 and O-GlcN acylation in breast cancer. Molecular Cancer Research *13*. 10.1158/1541-
1128 7786.MCR-14-0536.

1129 94. Kuo, Y., Huang, H., Cai, T., and Wang, T. (2015). Target of rapamycin complex 2
1130 regulates cell growth via Myc in drosophila. Sci Rep *5*. 10.1038/srep10339.

1131 95. Miyahara, H., Yadavilli, S., Natsumeda, M., Rubens, J.A., Rodgers, L., Kambhampati,
1132 M., Taylor, I.C., Kaur, H., Asnaghi, L., Eberhart, C.G., et al. (2017). The dual mTOR
1133 kinase inhibitor TAK228 inhibits tumorigenicity and enhances radiosensitization in
1134 diffuse intrinsic pontine glioma. Cancer Lett *400*. 10.1016/j.canlet.2017.04.019.

1135 96. Flannery, P.C., DeSisto, J.A., Amani, V., Venkataraman, S., Lemma, R.T., Prince,
1136 E.W., Donson, A., Moroze, E.E., Hoffman, L., Levy, J.M.M., et al. (2018). Preclinical
1137 analysis of MTOR complex 1/2 inhibition in diffuse intrinsic pontine glioma. Oncol
1138 Rep *39*. 10.3892/or.2017.6122.

1139 97. Schlee, M., Schuhmacher, M., Hölzel, M., Laux, G., and Bornkamm, G.W. (2007). c-
1140 MYC Impairs Immunogenicity of Human B Cells. Adv Cancer Res *97*.
1141 10.1016/S0065-230X(06)97007-9.

1142 98. Jones, P.A., Ohtani, H., Chakravarthy, A., and De Carvalho, D.D. (2019). Epigenetic
1143 therapy in immune-oncology. Nat Rev Cancer *19*. 10.1038/s41568-019-0109-9.

1144 99. See, Y.X., Chen, K., and Fullwood, M.J. (2022). MYC overexpression leads to
1145 increased chromatin interactions at super-enhancers and MYC binding sites. Genome
1146 Res *32*. 10.1101/gr.276313.121.

1147 100. Jaitin, D.A., Kenigsberg, E., Keren-Shaul, H., Elefant, N., Paul, F., Zaretsky, I.,
1148 Mildner, A., Cohen, N., Jung, S., Tanay, A., et al. (2014). Massively parallel single-
1149 cell RNA-seq for marker-free decomposition of tissues into cell types. Science (1979)
1150 *343*. 10.1126/science.1247651.

1151 101. Keren-Shaul, H., Kenigsberg, E., Jaitin, D.A., David, E., Paul, F., Tanay, A., and
1152 Amit, I. (2019). MARS-seq2.0: an experimental and analytical pipeline for indexed
1153 sorting combined with single-cell RNA sequencing. Nat Protoc *14*. 10.1038/s41596-
1154 019-0164-4.

1155 102. Meers, M.P., Bryson, T.D., Henikoff, J.G., and Henikoff, S. (2019). Improved cut&run
1156 chromatin profiling tools. Elife *8*. 10.7554/ELIFE.46314.

1157 103. Blecher-Gonen, R., Barnett-Itzhaki, Z., Jaitin, D., Amann-Zalcenstein, D., Lara-
1158 Astiaso, D., and Amit, I. (2013). High-throughput chromatin immunoprecipitation for
1159 genome-wide mapping of in vivo protein-DNA interactions and epigenomic states. Nat
1160 Protoc *8*. 10.1038/nprot.2013.023.

1161 104. Venkatesh, H.S., Morishita, W., Geraghty, A.C., Silverbush, D., Gillespie, S.M., Arzt,
1162 M., Tam, L.T., Espenel, C., Ponnuswami, A., Ni, L., et al. (2019). Electrical and
1163 synaptic integration of glioma into neural circuits. Nature *573*. 10.1038/s41586-019-
1164 1563-y.

1165 105. Martin, M. (2011). Cutadapt removes adapter sequences from high-throughput
1166 sequencing reads. EMBnet J *17*. 10.14806/ej.17.1.200.

1167 106. Langmead, B., and Salzberg, S.L. (2012). Fast gapped-read alignment with Bowtie 2.
1168 Nat Methods *9*. 10.1038/nmeth.1923.

1169 107. Yu, G., Wang, L.G., and He, Q.Y. (2015). ChIP seeker: An R/Bioconductor package
1170 for ChIP peak annotation, comparison and visualization. Bioinformatics *31*.
1171 10.1093/bioinformatics/btv145.

1172 108. Shen, L., Shao, N., Liu, X., and Nestler, E. (2014). Ngs.plot: Quick mining and
1173 visualization of next-generation sequencing data by integrating genomic databases.
1174 BMC Genomics *15*. 10.1186/1471-2164-15-284.

1175 109. McLean, C.Y., Bristor, D., Hiller, M., Clarke, S.L., Schaar, B.T., Lowe, C.B., Wenger,
1176 A.M., and Bejerano, G. (2010). GREAT improves functional interpretation of cis-
1177 regulatory regions. Nat Biotechnol *28*. 10.1038/nbt.1630.

1178 110. Ramírez, F., Ryan, D.P., Grüning, B., Bhardwaj, V., Kilpert, F., Richter, A.S., Heyne,
1179 S., Dündar, F., and Manke, T. (2016). deepTools2: a next generation web server for
1180 deep-sequencing data analysis. Nucleic Acids Res *44*. 10.1093/NAR/GKW257.

1181 111. Quinlan, A.R., and Hall, I.M. (2010). BEDTools: A flexible suite of utilities for
1182 comparing genomic features. Bioinformatics *26*. 10.1093/bioinformatics/btq033.

1183 112. Fishilevich, S., Nudel, R., Rappaport, N., Hadar, R., Plaschkes, I., Stein, T.I., Rosen,
1184 N., Kohn, A., Twik, M., Safran, M., et al. (2017). GeneHancer: Genome-wide
1185 integration of enhancers and target genes in GeneCards. Database *2017*.
1186 10.1093/database/bax028.

1187 113. Kohen, R., Barlev, J., Hornung, G., Stelzer, G., Feldmesser, E., Kogan, K., Safran, M.,
1188 and Leshkowitz, D. (2019). UTAP: User-friendly Transcriptome Analysis Pipeline.
1189 BMC Bioinformatics *20*. 10.1186/s12859-019-2728-2.

1190 114. Dobin, A., Davis, C.A., Schlesinger, F., Drenkow, J., Zaleski, C., Jha, S., Batut, P.,
1191 Chaisson, M., and Gingeras, T.R. (2013). STAR: Ultrafast universal RNA-seq aligner.
1192 Bioinformatics *29*. 10.1093/bioinformatics/bts635.

1193 115. Anders, S., Pyl, P.T., and Huber, W. (2015). HTSeq-A Python framework to work
1194 with high-throughput sequencing data. Bioinformatics *31*.
1195 10.1093/bioinformatics/btu638.

1196 116. Love, M.I., Huber, W., and Anders, S. (2014). Moderated estimation of fold change
1197 and dispersion for RNA-seq data with DESeq2. Genome Biol *15*. 10.1186/s13059-
1198 014-0550-8.

1199 117. Subramanian, A., Tamayo, P., Mootha, V.K., Mukherjee, S., Ebert, B.L., Gillette,
1200 M.A., Paulovich, A., Pomeroy, S.L., Golub, T.R., Lander, E.S., et al. (2005). Gene set
1201 enrichment analysis: A knowledge-based approach for interpreting genome-wide
1202 expression profiles. Proc Natl Acad Sci U S A *102*. 10.1073/pnas.0506580102.

1203 118. Mootha, V.K., Lindgren, C.M., Eriksson, K.F., Subramanian, A., Sihag, S., Lehar, J.,
1204 Puigserver, P., Carlsson, E., Ridderstråle, M., Laurila, E., et al. (2003). PGC-1α-
1205 responsive genes involved in oxidative phosphorylation are coordinately
1206 downregulated in human diabetes. Nat Genet *34*. 10.1038/ng1180.

1207 119. Liberzon, A., Birger, C., Thorvaldsdóttir, H., Ghandi, M., Mesirov, J.P., and Tamayo,
1208 P. (2015). The Molecular Signatures Database Hallmark Gene Set Collection. Cell
1209 Syst *1*. 10.1016/j.cels.2015.12.004.

1210 120. Wiederschain, D., Chen, L., Johnson, B., Bettano, K., Jackson, D., Taraszka, J., Wang,
1211 Y.K., Jones, M.D., Morrissey, M., Deeds, J., et al. (2007). Contribution of Polycomb
1212 Homologues Bmi-1 and Mel-18 to Medulloblastoma Pathogenesis. Mol Cell Biol *27*.
1213 10.1128/mcb.02244-06.

1214 121. Van Staveren, W.C.G., Solís, D.W., Delys, L., Venet, D., Cappello, M., Andry, G.,
1215 Dumont, J.E., Libert, F., Detours, V., and Maenhaut, C. (2006). Gene expression in
1216 human thyrocytes and autonomous adenomas reveals suppression of negative
1217 feedbacks in tumorigenesis. Proc Natl Acad Sci U S A *103*.
1218 10.1073/pnas.0507354102.

1219 122. Wei, G., Twomey, D., Lamb, J., Schlis, K., Agarwal, J., Stam, R.W., Opferman, J.T.,
1220 Sallan, S.E., den Boer, M.L., Pieters, R., et al. (2006). Gene expression-based
1221 chemical genomics identifies rapamycin as a modulator of MCL1 and glucocorticoid
1222 resistance. Cancer Cell *10*. 10.1016/j.ccr.2006.09.006.

1223 123. Kuleshov, M. V., Jones, M.R., Rouillard, A.D., Fernandez, N.F., Duan, Q., Wang, Z.,
1224 Koplev, S., Jenkins, S.L., Jagodnik, K.M., Lachmann, A., et al. (2016). Enrichr: a
1225 comprehensive gene set enrichment analysis web server 2016 update. Nucleic Acids
1226 Res *44*. 10.1093/nar/gkw377.

1227 124. Keenan, A.B., Torre, D., Lachmann, A., Leong, A.K., Wojciechowicz, M.L., Utti, V.,
1228 Jagodnik, K.M., Kropiwnicki, E., Wang, Z., and Ma'ayan, A. (2019). ChEA3:
1229 transcription factor enrichment analysis by orthogonal omics integration. Nucleic
1230 Acids Res *47*. 10.1093/nar/gkz446.

1231 125. Dunham, I., Kundaje, A., Aldred, S.F., Collins, P.J., Davis, C.A., Doyle, F., Epstein,
1232 C.B., Frietze, S., Harrow, J., Kaul, R., et al. (2012). An integrated encyclopedia of
1233 DNA elements in the human genome. Nature *489*. 10.1038/nature11247.

1234 126. Raudvere, U., Kolberg, L., Kuzmin, I., Arak, T., Adler, P., Peterson, H., and Vilo, J.
1235 (2019). G:Profiler: A web server for functional enrichment analysis and conversions of
1236 gene lists (2019 update). Nucleic Acids Res *47*. 10.1093/nar/gkz369.

1237 127. Kanehisa, M. (2019). Toward understanding the origin and evolution of cellular
1238 organisms. Protein Science *28*. 10.1002/pro.3715.

1239 128. Kanehisa, M., and Goto, S. (2000). KEGG: Kyoto Encyclopedia of Genes and
1240 Genomes. Nucleic Acids Res *28*. 10.1093/nar/28.1.27.

129. Martens, M., Ammar, A., Riutta, A., Waagmeester, A., Slenter, D.N., Hanspers, K., Miller, R.A., Digles, D., Lopes, E.N., Ehrhart, F., et al. (2021). WikiPathways: Connecting communities. Nucleic Acids Res *49*. 10.1093/nar/gkaa1024.

130. Erratum: SynergyFinder 2.0: Visual analytics of multi-drug combination synergies (Nucleic Acids Research (2020) 48:W1 (W488-W493) DOI: 10.1093/nar/gkaa216) (2022). Nucleic Acids Res *50*. 10.1093/nar/gkac552.

131. Bankhead, P., Loughrey, M.B., Fernández, J.A., Dombrowski, Y., McArt, D.G., Dunne, P.D., McQuaid, S., Gray, R.T., Murray, L.J., Coleman, H.G., et al. (2017). QuPath: Open source software for digital pathology image analysis. Sci Rep *7*. 10.1038/s41598-017-17204-5.

132. Schmidt, U., Weigert, M., Broaddus, C., and Myers, G. (2018). Cell detection with star-convex polygons. In Lecture Notes in Computer Science (including subseries Lecture Notes in Artificial Intelligence and Lecture Notes in Bioinformatics) 10.1007/978-3-030-00934-2_30.

133. Shema, E., Jones, D., Shoresh, N., Donohue, L., Ram, O., and Bernstein, B.E. (2016). Single-molecule decoding of combinatorially modified nucleosomes. Science (1979) *352*. 10.1126/science.aad7701.

Figure 1

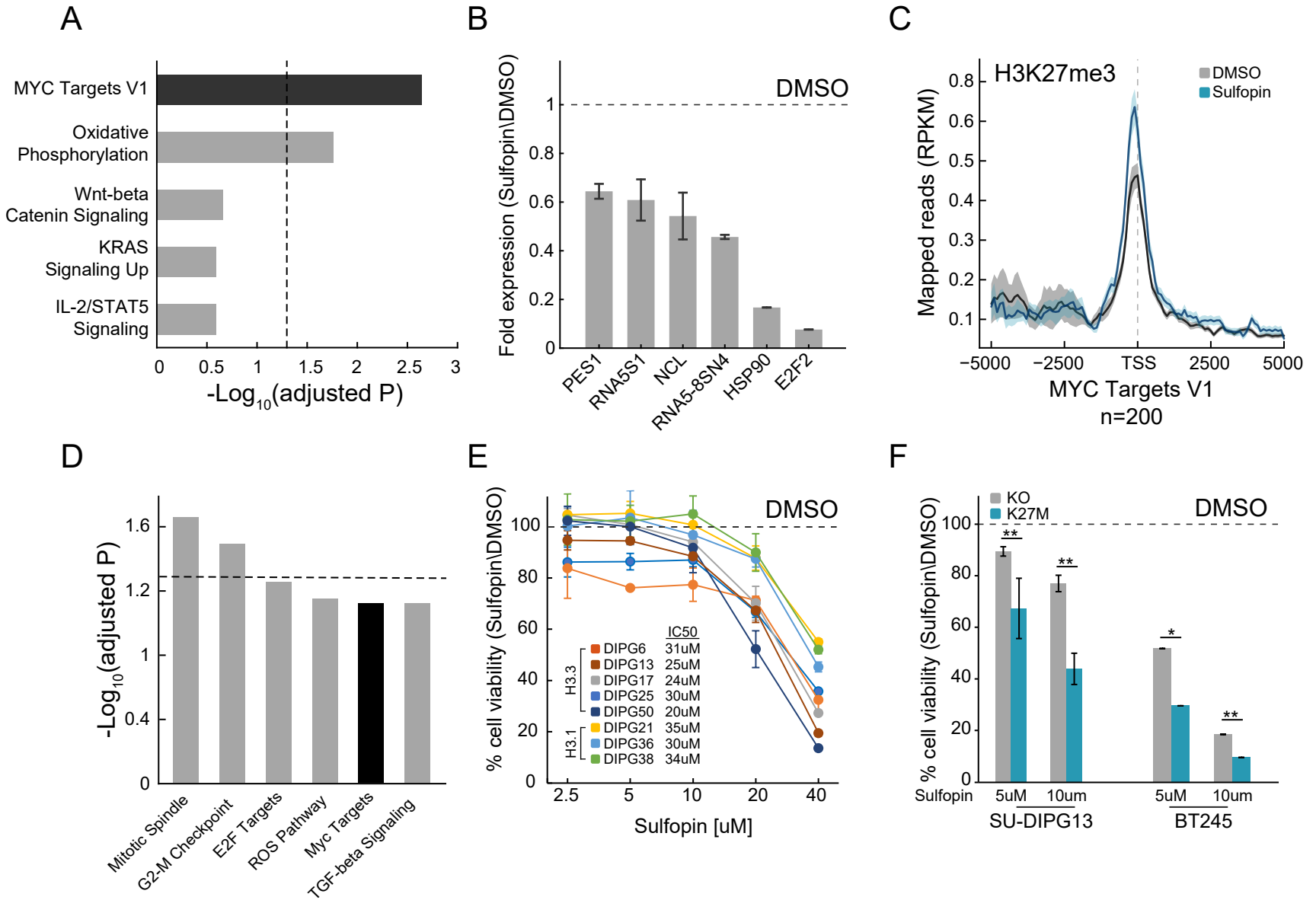
A
MYC Targets V1
Oxidative Phosphorylation
Wnt-beta Catenin Signaling
KRAS Signaling Up
IL-2/STAT5 Signaling
0
0.5
1
1.5
2
2.5
3
-Log10(adjusted P)
B
DMSO
Fold expression (Sulfopin\DMSO)
1
0.8
0.6
0.4
0.2
0
PES1
RNA5S1
NCL
RNA5-8SN4
HSP90
E2F2
C
H3K27me3
DMSO
Sulfopin
Mapped reads (RPKM)
0.8
0.6
0.5
0.4
0.3
0.2
0.1
−5000
−2500
TSS
2500
5000
MYC Targets V1
n=200
D
-Log10(adjusted P)
1.6
1.2
1
0.4
0
Mitotic Spindle
G2-M Checkpoint
E2F Targets
ROS Pathway
Myc Targets
TGF-beta Signaling
E
DMSO
% cell viability (Sulfopin\DMSO)
100
80
60
40
20
0
IC50
H3.3
DIPG6 31uM
DIPG13 25uM
DIPG17 24uM
DIPG25 30uM
DIPG50 20uM
H3.1
DIPG21 35uM
DIPG36 30uM
DIPG38 34uM
2.5
5
10
20
40
Sulfopin [uM]
F
KO
K27M
DMSO
% cell viability (Sulfopin\DMSO)
100
80
60
40
20
0
**
**
*
**
Sulfopin
5uM
10um
5uM
10um
SU-DIPG13
BT245

Figure 2

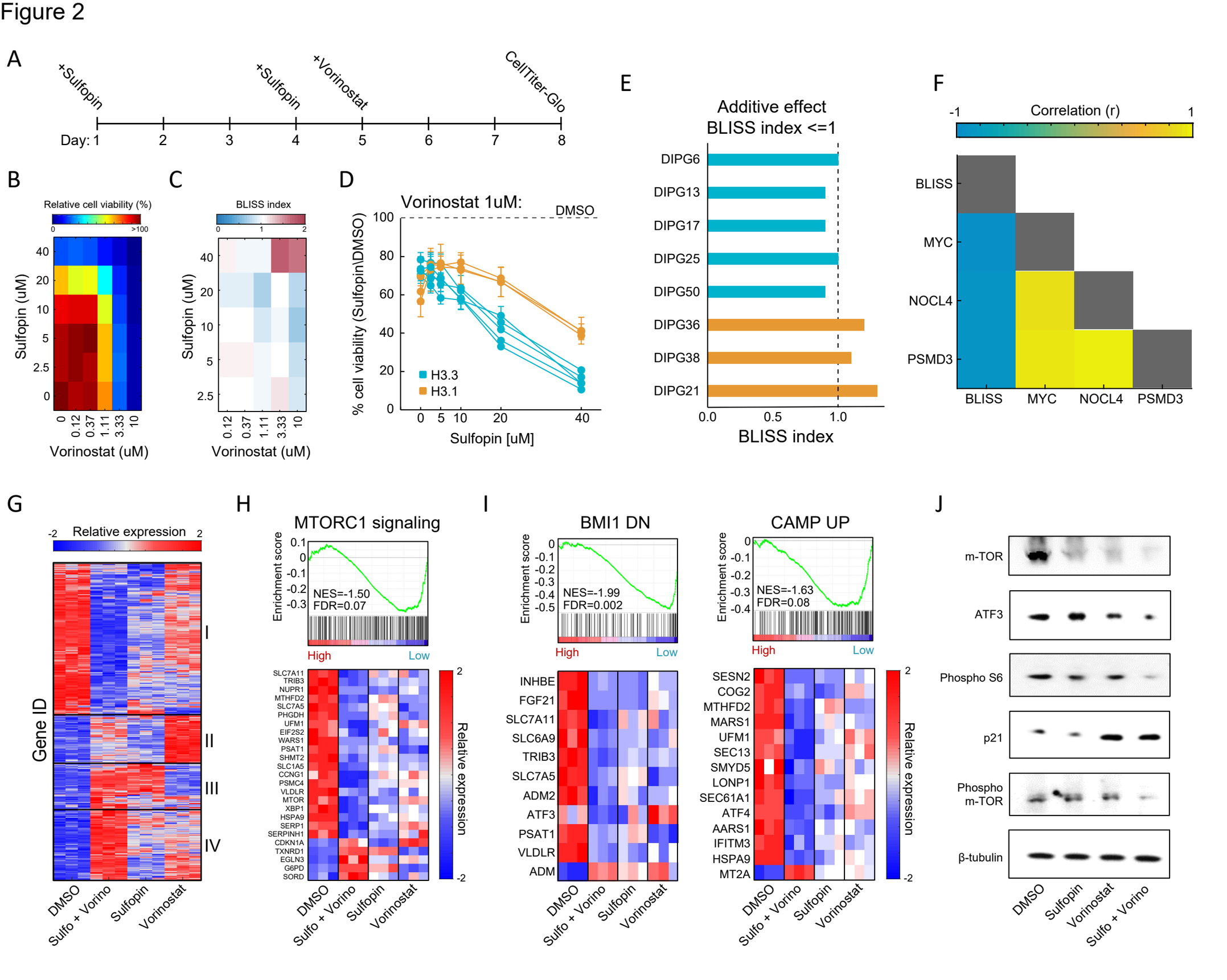
A
+Sulfopin
+Sulfopin
+Vorinostat
CellTiter-Glo
Day: 1 2 3 4 5 6 7 8
B
Relative cell viability (%)
0 >100
Sulfopin (uM)
40 20 10 5 2.5 0
0 0.12 0.37 1.11 3.33 10
Vorinostat (uM)
C
BLISS index
0 1 2
Sulfopin (uM)
40 20 10 5 2.5
0.12 0.37 1.11 3.33 10
Vorinostat (uM)
D
Vorinostat 1uM:
DMSO
% cell viability (Sulfopin\DMSO)
100 80 60 40 20 0
H3.3
H3.1
0 5 10 20 40
Sulfopin [uM]
E
Additive effect
BLISS index <=1
DIPG6
DIPG13
DIPG17
DIPG25
DIPG50
DIPG36
DIPG38
DIPG21
0.0 0.5 1.0
BLISS index
F
-1 Correlation (r) 1
BLISS
MYC
NOCL4
PSMD3
BLISS MYC NOCL4 PSMD3
G
-2 Relative expression 2
Gene ID
I
II
III
IV
DMSO
Sulfo + Vorino
Sulfopin
Vorinostat
H
MTORC1 signaling
Enrichment score
0.1 0 -0.1 -0.2 -0.3
NES=-1.50
FDR=0.07
High
Low
SLC7A11
TRIB3
NUPR1
MTHFD2
SLC7A5
PHGDH
UFM1
EIF2S2
WARS1
PSAT1
SHMT2
SLC1A5
CCNG1
PSMC4
VLDLR
MTOR
XBP1
HSPA9
SERP1
SERPINH1
CDKN1A
TXNRD1
EGLN3
G6PD
SORD
2
Relative expression
-2
DMSO
Sulfo + Vorino
Sulfopin
Vorinostat
I
BMI1 DN
Enrichment score
0 -0.1 -0.2 -0.3 -0.4 -0.5
NES=-1.99
FDR=0.002
High
Low
INHBE
FGF21
SLC7A11
SLC6A9
TRIB3
SLC7A5
ADM2
ATF3
PSAT1
VLDLR
ADM
CAMP UP
Enrichment score
0 -0.1 -0.2 -0.3 -0.4
NES=-1.63
FDR=0.08
High
Low
SESN2
COG2
MTHFD2
MARS1
UFM1
SEC13
SMYD5
LONP1
SEC61A1
ATF4
AARS1
IFITM3
HSPA9
MT2A
2
Relative expression
-2
DMSO
Sulfo + Vorino
Sulfopin
Vorinostat
J
m-TOR
ATF3
Phospho S6
p21
Phospho m-TOR
β-tubulin
DMSO
Sulfopin
Vorinostat
Sulfo + Vorino

Figure 3

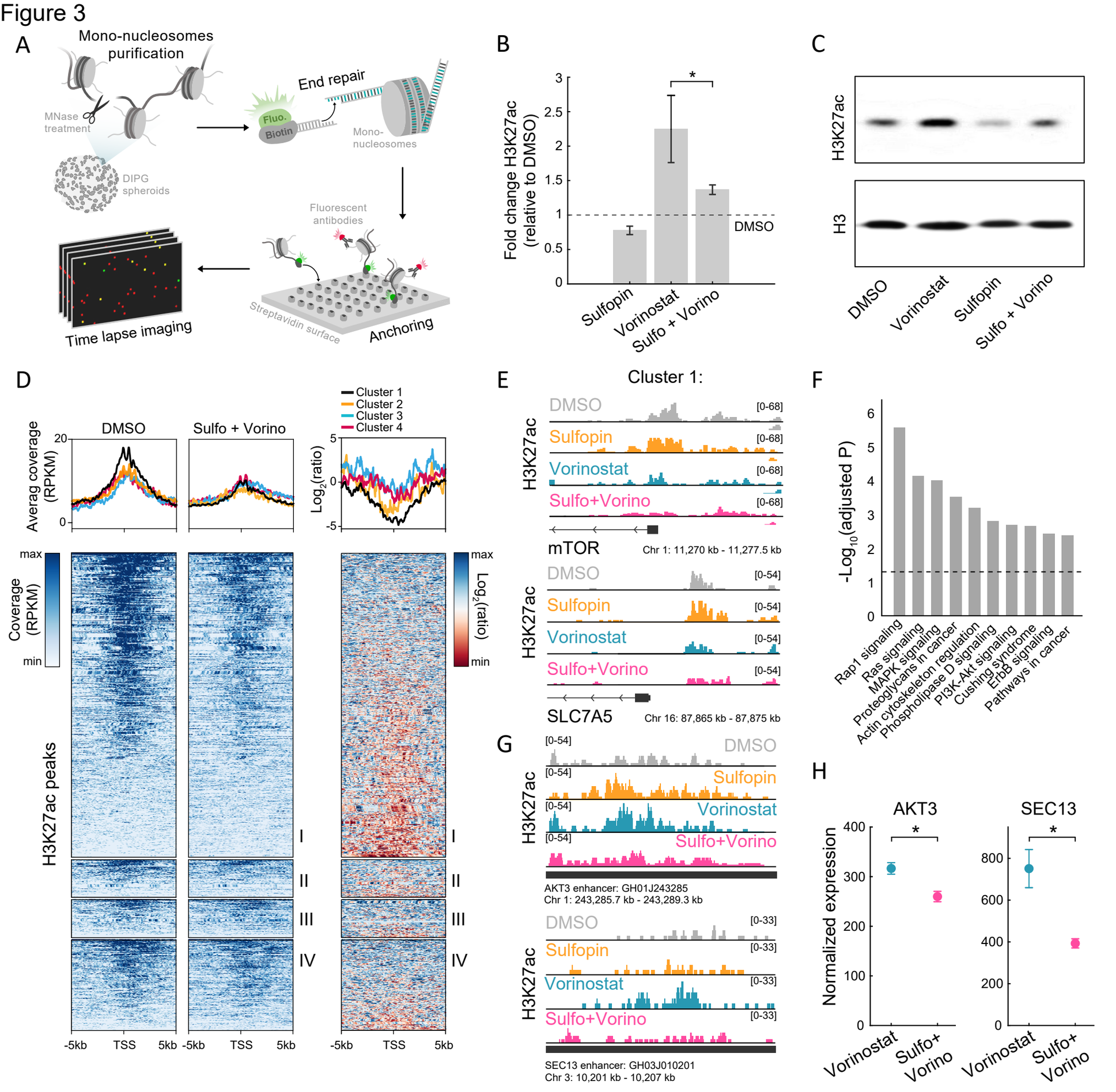
A
Mono-nucleosomes purification
MNase treatment
DIPG spheroids
End repair
Fluo.
Biotin
Mono-nucleosomes
Fluorescent antibodies
Streptavidin surface
Anchoring
Time lapse imaging
B
Fold change H3K27ac (relative to DMSO)
DMSO
Sulfopin
Vorinostat
Sulfo + Vorino
C
H3K27ac
H3
DMSO
Vorinostat
Sulfopin
Sulfo + Vorino
D
Cluster 1
Cluster 2
Cluster 3
Cluster 4
DMSO
Sulfo + Vorino
Averag coverage (RPKM)
Log2(ratio)
Coverage (RPKM)
max
min
H3K27ac peaks
I
II
III
IV
-5kb
TSS
5kb
E
Cluster 1:
H3K27ac
DMSO
Sulfopin
Vorinostat
Sulfo+Vorino
mTOR
Chr 1: 11,270 kb - 11,277.5 kb
SLC7A5
Chr 16: 87,865 kb - 87,875 kb
F
-Log10(adjusted P)
Rap1 signaling
Ras signaling
MAPK signaling
Proteoglycans in cancer
Actin cytoskeleton regulation
Phospholipase D signaling
PI3K-Akt signaling
Cushing syndrome
ErbB signaling
Pathways in cancer
G
AKT3 enhancer: GH01J243285
Chr 1: 243,285.7 kb - 243,289.3 kb
SEC13 enhancer: GH03J010201
Chr 3: 10,201 kb - 10,207 kb
H
AKT3
SEC13
Normalized expression
Vorinostat
Sulfo+ Vorino

Figure 4

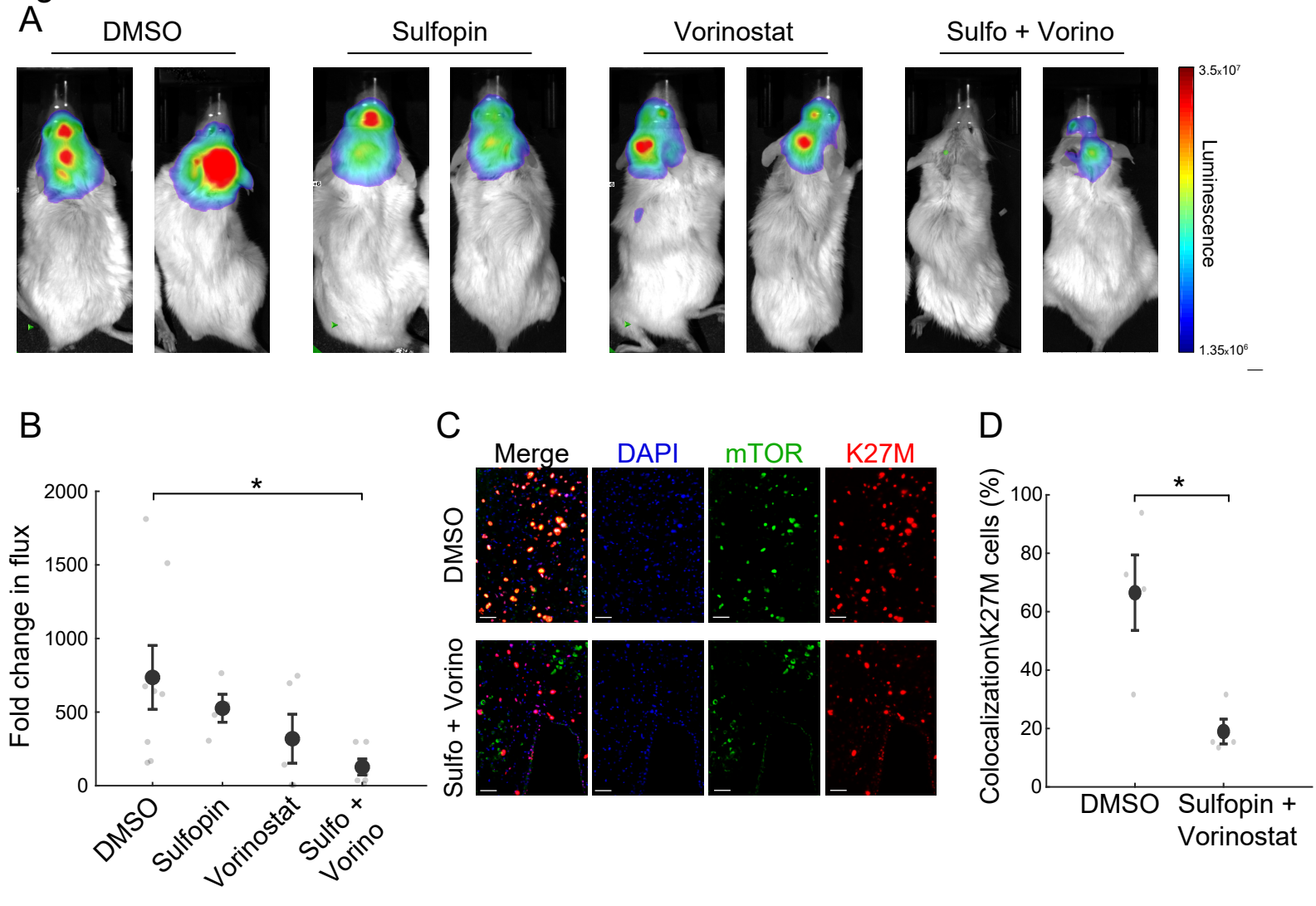
A
DMSO
Sulfopin
Vorinostat
Sulfo + Vorino
3.5x10^7
Luminescence
1.35x10^6
B
Fold change in flux
2000
1500
1000
500
0
*
DMSO
Sulfopin
Vorinostat
Sulfo + Vorino
C
Merge
DAPI
mTOR
K27M
DMSO
Sulfo + Vorino
D
Colocalization\K27M cells (%)
100
80
60
40
20
0
*
DMSO
Sulfopin + Vorinostat